

Downconversion Materials for Perovskite Solar Cells

Ram Datt, Swati Bishnoi, Declan Hughes, Prerna Mahajan, Anoop Singh, Ramashanker Gupta, Sandeep Arya, Vinay Gupta, and Wing Chung Tsoi*

Perovskite solar cells (PSCs) have made game-changing progress in the last decade and reached a power conversion efficiency (PCE) of up to 25%. Furthermore, the development of material chemistry, structure design, active layer composition, process engineering, etc. has contributed to improving PSCs' stability. The significant PCE losses experienced by PSCs are related to spectral mismatch between the incident solar spectra and absorption range of the active layer, which thereby limits the PCE. Besides PSCs' performance, the photoinduced degradation is also a major concern. Recently, lanthanide (rare-earth) and nonlanthanide-based downconversion (DC) materials have been introduced to resolve these spectral mismatch losses as well as reduce the photoinduced degradation. The DC materials improve the photovoltaic performance by converting ultraviolet (UV) light to visible, also providing UV shielding, and thus contribute to increasing the efficiency as well as stability of PSCs. Moreover, the Shockley–Queisser efficiency limit of the solar cell can be crossed with the help of DC materials. In this review, the importance, processing, and the reported DC materials for PSCs are thoroughly discussed. Furthermore, the development of DC materials and their impact on PSCs' performance and stability, along with their future perspectives, are focused.

supply, society needs to consider alternative renewable energy sources. Out of the various available renewable energy sources, solar energy is one of the most abundant, efficient, and ecofriendly resources, which can meet the global energy demand.^[2,3] In photovoltaic technology, perovskite solar cells (PSCs) have lately emerged as an inexpensive, solution-processable, versatile, and reliable option with improved performance compared with already existing inorganic photovoltaic technologies. PSCs have attained enormous research curiosity due to organo-lead halide perovskite materials having favorable optoelectronic properties such as a high absorption coefficient, high charge carrier mobilities, low trap density, extended carrier recombination time, etc.^[4–8] In 2009, a major breakthrough was achieved in PSCs after the introduction of organometal halide perovskites as visible light sensitizers.^[9] Furthermore, the power conversion efficiency (PCE) of PSCs has been reported to be enhanced by more than 25% within

one decade.^[10,11] Besides PCE, the cost and lifetime of devices are the other foremost requirements for technological commercialization. Material engineering can deliver a promising strategy to achieve stable photovoltaic devices. The mixed-halide perovskite photoactive layers were reported to be stable compared with single-halide-based PSC devices in ambient conditions.^[12] The doping of bromide and cesium can improve the stability of well-reported thin-film methylammonium lead iodide perovskite ($\text{CH}_3\text{NH}_3\text{PbI}_3$) in humid air environment and the tuning of the

1. Introduction

Energy is the lifeblood of modern society, powering everything from our homes to our communication networks, transportation, and industrial endeavors. These days, the ability of humans to survive depends more on the availability of energy. Energy consumption and carbon emissions are increasing, and it is expected both will double by 2050 compared with their 2001 levels.^[1] As we are reliant on fossil fuels (nonrenewable), which have a finite

R. Datt, D. Hughes, W. C. Tsoi
SPECIFIC
Faculty of Science and Engineering
Swansea University
Swansea SA1 8EN, UK
E-mail: w.c.tsoi@swansea.ac.uk

S. Bishnoi
Department of Chemical Engineering
Indian Institute of Technology, Delhi
New Delhi 110016, India

P. Mahajan, A. Singh, S. Arya
Department of Physics
University of Jammu
Jammu, Jammu and Kashmir 180006, India

R. Gupta
Advanced Materials and Devices Metrology Division
CSIR-National Physical Laboratory
New Delhi 110012, India

V. Gupta
Department of Physics
Khalifa University of Science and Technology
Abu Dhabi 127788, UAE

 The ORCID identification number(s) for the author(s) of this article can be found under <https://doi.org/10.1002/solr.202200266>.

© 2022 The Authors. Solar RRL published by Wiley-VCH GmbH. This is an open access article under the terms of the Creative Commons Attribution License, which permits use, distribution and reproduction in any medium, provided the original work is properly cited.

DOI: 10.1002/solr.202200266

tolerance factor has also shown improvement in the perovskite structure.^[13–15] Unfortunately, PSCs are lacking in long-term stability as organic–inorganic halide perovskite materials are sensitive to moisture and oxygen, which causes instability due to perovskite layer degradation.^[16–20] Major environmental-deteriorating variables including humidity and oxygen can be fixed by encapsulation. The light-induced degradation is still a challenge for PSCs, and its different causes are being reported. However, UV light is the most destructive reason for affecting stability. UV light decomposes the perovskite layer as well as induces vacancies and oxygen defects that deplete the PSCs' performance.^[21] On the other hand, the photocatalytic properties of the electron transport layer (ETL) result in charge carrier recombination at the ETL/perovskite interface layer and are also responsible for poor device performance.^[22,23] Besides this, long-term irradiation of UV light upon ETL (titanium dioxide (TiO₂)) can produce oxygen vacancies that create the deep trap state at the ETL surface and contribute to recombination losses of photogenerated charge carriers.^[24,25] Meanwhile, the photogenerated holes in the ETL (TiO₂) surface can react with iodine (I) ions and cause CH₃NH₃PbI₃ layer decomposition and degrade the performance of PSC devices.^[26,27] These issues have been addressed by various researchers, and they proposed replacement of a well-tested material like TiO₂ as the ETL with other materials such as zinc oxide (ZnO), tin oxide (SnO₂), cadmium sulfide (CdS), chromium oxide (Cr₂O₃), strontium titanate (SrTiO₃), barium stannate (BaSnO₃), zinc tin oxide (Zn₂SnO₄), etc.^[28–34] In addition, three different significant techniques were proposed for addressing the issue of PSCs' instability under UV irradiation, such as removing the mesoporous TiO₂ layer, protecting the mesoporous TiO₂ layer from UV light, and TiO₂ surface states passivation.^[35] The incident AM1.5 G spectrum has been further utilized through the use of tandem PSCs and can achieve high PCE.^[36–38] In the tandem structure, the two different bandgap perovskite absorber layers are fabricated and connected through an interlayer.^[39,40] This improves the utilization of the visible-to-near-infrared (NIR) incident solar spectrum light. Despite all these approaches, the PSCs' stability under UV irradiation and utilization of high-energy incident solar spectrum could not be resolved, which is undoubtedly an important reason for the limited stability and efficiency of devices. The perovskite material shows an enormous absorption coefficient in the UV-blue region of the order of 10⁵ cm⁻¹, which is comparatively higher than the visible region.^[41,42] Unfortunately, the UV-blue region does not contribute to improving the PSCs' performance and also causes degradation within the active layer (AL).^[43] There are many mechanisms proposed for losses in the lower region, such as higher reflectance losses in the short-wavelength region (due to the refractive index mismatch of air and the fluorine-doped tin oxide [FTO] substrate).^[44–46] With downconversion (DC) materials, the spectral response improved at lower wavelengths, thereby suggesting good spectral matching. Interestingly, the DC-based devices show better efficiency under continuous illumination compared with control devices. The degradation occurs due to different environmental factors such as oxygen, water, light, and temperature, which are classified as external factors. The internal factors affecting the lifetime of PSCs are the structure and composition of the perovskite light-absorbing layer, buffer layer traps and morphology,

perovskite/buffer layer and perovskite/electrode interface interaction, and the types of charge extraction materials along with the device structure.^[47–52] The use of inorganic charge extraction layers was claimed to increase the stability (≈1000 h). However, this is not long enough to ensure long-term stability.^[53,54] The charge extraction layer and perovskite interface charge-trapped states are also responsible for device degradation,^[55] especially, the TiO₂ electron extraction layer-based devices, which are degraded rapidly under light soaking and therefore harm the long-term device stability.^[56] Sun et al.^[57] illustrated that the oxygen-rich environment can affect the microstructure and electronic quality of the perovskite film that ultimately hinders the long-term stability. They highlighted that the oxygen-induced photodegradation was initiated from grain boundaries and continued to extend into the interior of grains and penetrated the whole film. Zhang et al.^[58] further suggested that this may be due to the grain boundary region which is rich in defect density. Rahman et al.^[21] explained that the DC-based devices maintains the favorable perovskite film morphology and helped to reduce the traps. Also, after being exposed to a high-humidity environment (relative humidity (RH): 85–90%, 25 °C), there is an improvement in long-term stability. The perovskite film coated on the DC layer forms a smoother layer in comparison with the TiO₂ layer. Chen et al.^[59] also reported the improvement of the PSCs' device stability in the dark environment after introducing the DC material on top of the TiO₂ layer. Moreover, the incorporation of DC material into the perovskite facilitates sensitization, light scattering, enlarges grain size and improve perovskite film crystallinity, therefore enhancing the PSCs' performance and stability.^[60–62] Under UV exposure, the long-term ambient stability is also enhanced by improving the crystallinity of the perovskite film after doping with DC material.^[63] DC materials doping into perovskite also improves the charge carrier lifetimes and leads to efficiency enhancement of PSCs.^[64–66] Besides this, DC materials doping also contributes to preferable energy-level alignment and also diminishes trap-state density in PSCs.^[67–69] Moreover, DC materials doping aids the development of perovskite grains with lesser defects.^[70] Currently, solar cells include spectrum conversion layers to facilitate the conversion of higher to lower photon energy and vice versa, known as DC and upconversion (UC) processes, respectively. The UC mechanism enables utilization of the incident NIR solar spectrum in the PSCs, which otherwise remains unutilized. UC materials with unique energy-level structuring have the potential to enhance the absorbance spectra of PSCs up to NIR. UC materials can sequentially absorb two low-energy photons (NIR) and emit a high-energy photon (visible). Thus, they have been researched widely for PSCs to overcome nonabsorption loss, thereby improving their resultant efficiency.^[71–73] The maximum efficiency of solar cells is theoretically calculated to be 30% for a 1.1 eV bandgap AL when taking radiative recombination into consideration and is defined as the detailed balance limit or Shockley–Queisser (SQ) limit of efficiency.^[74] The short absorption region of the solar cells causes lower PCE, and the high-energy region triggers thermalization losses within the AL. The convertor materials have been suggested to improve the efficiency of the existing solar cells and may even assist in exceeding the SQ limit.^[75] The enhancement of solar cell efficiency through the concept of photon-induced transitions at

intermediate levels and carrier multiplication was discussed in detail by Antonio Luque et al.^[76] and Rolf Brendel et al.^[77] respectively. The DC mechanism was additionally proposed for incident solar spectral modification for solar cell development at the material level.^[78] In recent years, DC materials have been investigated for solar cell devices to improve the utilization of high-energy photons and aid in the minimization of thermalization losses. In the DC process, one lanthanide ion (donor) transmits excited energy to two additional lanthanide ions (acceptors) in a sequential manner. Forster and Dexter^[79,80] described the theory relating to energy transfer rate and the model for donor–acceptor interactions. The perovskite materials and their application in solar cells using different device structures and interlayers modification have been well reviewed.^[81–87] In this review, the main focus is given on the overview of DC materials mechanism, their implementation methods in PSCs, PCE improvement, and the impact of DC materials on device stability. This article also contains the material composite details of lanthanide and nonlanthanide-based DC materials used for PSCs. Furthermore, the review also highlights the current challenges and future prospectives of DC materials for PSCs.

1.1. Lanthanide DC Materials

Lanthanides are a series of 15 chemical elements found within the *f*-block of the periodic table. These elements have atomic numbers (*Z*) from 57 to 71 and also include scandium (*Z* = 21) and yttrium (*Z* = 39). Lanthanides consist of elements that follow lanthanum and involve the filling of 4*f* electronic subshell. Although lanthanum, scandium, and yttrium do not fill the 4*f* subshell, their properties behave as lanthanides. Lanthanides are also popularly known as rare-Earth (RE) elements and become important due to their unique optical, magnetic, and catalytic properties. Luminescence is the heart of lanthanides and thus is a promising class of materials, for applications such as lighting, electronic displays, light-emitting diodes (LEDs), sensors, lasers, security inks, etc.^[88,89] Therefore, photoluminescence is an attractive property of lanthanides and exhibits sharp emission peaks with high color purity. Lanthanides however do not possess high photoluminescence intensity due to these materials having weak light absorption.^[90] Luminescence intensity is directly proportional to absorbed light, and weak absorption of the lanthanide influences the output photoluminescence. The sensitization (antenna effect) mechanism is a well-known phenomenon adopted for lanthanide ions to overcome their weak absorption issue and modify the luminescence properties accordingly. The emission colors mainly depend on lanthanide ions as well as the surrounding environment. The luminescence is the result of the radiative and nonradiative transition of an electronically excited ion. The lanthanide atoms have the same number of valence electrons in the outermost shell for all the species, whereas 4*f* orbitals are progressively filled with increasing atomic number. The filling of 4*f* orbitals is related to the chemical and physical properties of elements. These 4*f* orbitals are shielded from the electrons in the 4*s* and 5*p* shells. This shielding helps for many useful properties of lanthanide ions such as narrowband emission, luminescence, and excited-state longer lifetime. Eu^{III}, Gd^{III}, and Tb^{III} are among the popular choices for synthesizing luminescent materials to generate

luminescence in the visible region with respect to the energy gap requirement. On the other hand, Eu³⁺ upon UV excitation emits two red photons called the DC effect.

1.2. Nonlanthanide DC Materials

The development of efficient DC materials for spectral conversion in PV cells is of great significance for enhancing their PCE, without altering their underlying architecture. As discussed, most of the DC materials are based on lanthanide and RE-based luminescent materials. Most RE materials have similar chemical properties and their process of separation, refinement, and purification is highly tedious and expensive.^[91] Despite this, the overall consumption of lanthanides has increased substantially over the past few years.^[92] This, coupled with a highly expensive and severely environmentally harmful mining/refining process, has led the research focus to the development of RE-free luminescent materials and in recent years several research groups have developed efficient lanthanide-free luminescent materials.^[93] The RE-free DC materials can be developed using four main strategies: 1) use of transition metals as luminescent centers,^[94] 2) generating defect-related luminescence, 3) utilizing self-luminescent materials such as tungstates and vanadates, and 4) luminescent quantum dots (QDs).

1.2.1. Transition Metals as Luminescent Centers

Besides lanthanides, certain transition metal elements-based complexes and coordination compounds show exceptional luminescent behavior. Coordination compounds of V, Cr, Mn, Fe, Co, Ni, and Cu are popular as luminescent materials. Manganese and vanadium are among the two comparatively abundant *d*-metal elements that exhibit luminescence at room temperature.

1.2.2. Defect-Related Luminescence

In recent years defect-related luminescent materials have attained specific research interest in silica-based materials, metal oxides, boron carbon oxynitride materials, phosphate-based compounds, and carbon-based compounds. The defect-related luminescence compounds are still a question of debate, but in most cases, it is attributed to vacancies, impurities, radical impurities, donor–acceptor pairs, etc.

1.2.3. Self-Activated Luminescent Materials

Another popular category is self-activated luminescent materials which exhibit luminescence without any activator ions. Vanadate materials are one of the most common materials in this category as they show charge transfer mechanism due to the presence of (VO₄)^{3−} clusters. Furthermore, vanadate-based self-luminescent compounds are low cost, require low calcination temperature, and have a broad emission spectrum. Similarly, tungstate and molybdate compounds also fall in the category of self-activated luminescence materials and the luminescent behavior is mainly attributed to charge transfer transition, defect recombination, and exciton emission.

1.2.4. Luminescent QDs

QDs of semiconducting nanocrystals are also another class of DC materials that shows tunable luminescence properties and offer certain advantages over traditional RE-based luminescence materials in terms of luminescence efficiency and color tunability. Moreover, due to the nanosized dimensions of QDs, the application domain is also large when compared with bulk luminescent materials. QDs of InP, CdSe, carbon, graphene, ZnO, and graphene phase (g-C3N4) are some of the commonly used materials in this category.

2. DC Materials and Their Properties for Solar Cells

The DC materials can absorb the high-energy photon (300–500 nm) and re-emit a longer-wavelength photon to which the photovoltaic (PV) device is more sensitive. Various types of DC materials have been investigated for this purpose like QDs, oxides, luminescent glasses, lanthanides, and organic dyes. Two major types of energy-conversion phenomena have been defined, known as down-shifting and DC, and both exhibit differences in their quantum efficiency (QE). The theoretical QE of downshifting shows less than unity, while DC has QE with greater or equal to unity.^[95] However, in practicality, this convention is not followed and the term DC is used for materials with a less-than-unity QE.^[96] In this review, the DC term has been used for reported materials. The DC materials can be used to overcome the poor blue response of solar cells. To maximize the efficiency of PV devices, the DC materials absorb short-wavelength light, typically in the 300–500 nm range, and re-emit it at a longer wavelength. A DC layer is typically applied directly to the front surface of a solar cell or doped into the charge transport layer (CTL) or photoactive layer to improve the device performance. **Figure 1** shows the schematic design of a DS or DC layer placed at the front side of the solar cell.

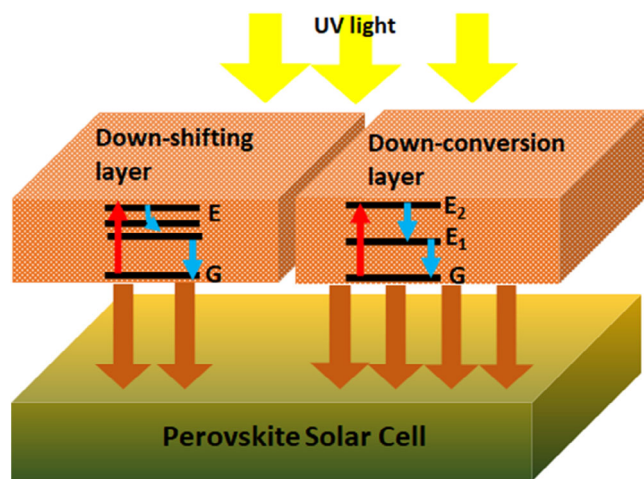


Figure 1. Schematic design of a solar cell device with luminescent down-shifting and DC layer directly placed onto the surface of the solar cell.

In PSCs, the absorption region covers the wavelength range from ≈ 300 to 850 nm, whereas the peak absorption intensity varies as per perovskite layer compositions.^[97] For example, in a $\text{CH}_3\text{NH}_3\text{PbI}_3$ perovskite layer, the estimated absorption coefficient is 1.5×10^4 and $0.5 \times 10^4 \text{ cm}^{-1}$ at 550 and 700 nm, respectively.^[6] Moreover, the mixed-halide perovskite films have shown different absorption properties and their absorption coefficients are dependent on the halide composition.^[12,98] For PSCs, the UV regions are unutilized and are also considered to be harmful to the devices. As a result, the first requirement for choosing a DC layer for PSCs is that their absorption must be in the UV range and should not overlap with the photoactive layer absorption. Their emission zone, on the other hand, should cover the photoactive layer's absorption peak.

2.1. Spectral Region Available for DC Materials for Photovoltaic Application

The spectral distribution (280–2500 nm, 0.5–4.4 eV) of sunlight at air mass 1.5 Global (AM 1.5 G) includes photons with a wide range of wavelengths ranging from UV to IR. The current generation of PV cells can only utilize a small fraction of the incident solar photons with sufficient energy and is consistent with the characteristic energy bandgap. **Figure 2** shows the solar spectral region available for DC materials.

This is attributed to the response each PV material has to a narrow range of solar photons with energy equal to the usual bandgap of the material. This bandgap varies from material to material. When the high-energy photon(s) are absorbed, the surplus energy (which is greater than the bandgap) is released as heat. This process is referred to as thermalization loss. In addition, photons with energy lower than the bandgap of the PV cell are not absorbed and are lost via transmission phenomena. In PSCs, the organic–inorganic materials used for the fabrication of the photoactive layer possess maximum absorption in the visible and NIR regions. The excess photon

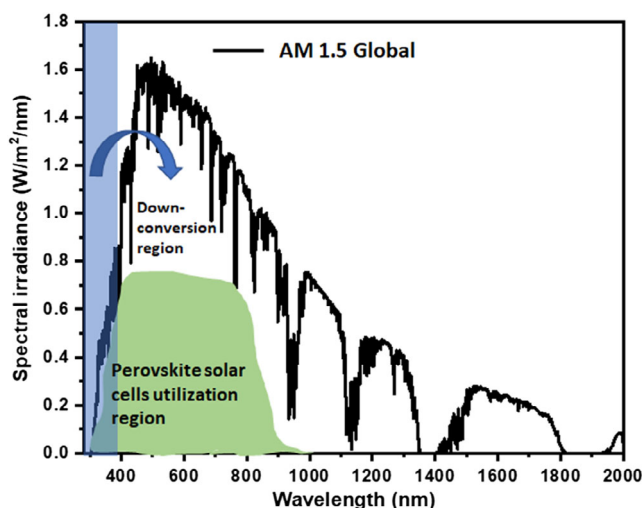


Figure 2. The AM 1.5 G spectrum where the portion (highlighted in green) is typically absorbed by a perovskite-based PV cell and the blue region is available for utilization by DC material spectral conversion.

energy of UV light is released as heat or simply not absorbed. However, the thermalization losses cannot simply be resolved using a large-bandgap material. The large-bandgap materials will help to reduce the thermalization losses, whereas, it will also limit the number of photons that can be absorbed across the spectrum. An attractive approach to reduce the thermalization losses and nonabsorption losses is to use luminescent materials as spectral converters.

3. DC Materials for PSCs

The three major known types of PSCs structures available, are planar conventional, inverted, and conventional with mesoporous structures, as shown in **Figure 3**.

The electron and hole transporting layers play a major role in avoiding direct contact between the substrate and the perovskite layer. The CTLs are primarily made up of inorganic semiconductor nanomaterials such as ZnO, TiO₂, SnO₂, etc. Moreover, the organic buffer layers are also applied in PSCs. The DC materials can either be introduced as dopants in the buffer (front electrode) or the mesoporous layer or on top of it or on the front side of the device, as shown in Figure 3. There are a variety of reports available in which researchers have introduced DC materials in PSCs by different ways.

3.1. Lanthanides DC Materials

A variety of lanthanide-based DC materials have been introduced in PSCs to achieve spectral conversion for improving their efficiency and stability.

3.1.1. Europium (Eu)-Based DC Materials

YVO₄:Eu³⁺: The Eu³⁺-doped yttrium vanadate (YVO₄) was first reported as DC by Chander et al.^[99] for PSCs application. The YVO₄:Eu³⁺ nanophosphor was demonstrated as a DC material and shows improvement in photovoltaic performance as well as in the stability of PSCs. YVO₄:Eu³⁺ has excitation and photoemission in UV and visible regions, respectively. This has made it a suitable material as a DC phosphor for PSCs. The photoluminescence spectra show a highly intensive peak at ≈625 nm for 11 mol% of Eu material at 295 nm excitation. In addition, the YVO₄:Eu³⁺ nanophosphor material has strong redlight emission, which is perfectly matched with the photoactive layer's absorption. After 2 h of measurement of DC-based devices, the measured short-circuit current (*J*_{sc}) retains 96% of its initial value as compared with 85% retention of the control devices.

YVO₄:Eu³⁺, Bi³⁺: The use of YVO₄:Eu³⁺ materials as spectral converters was previously studied.^[99] The doping of Bi³⁺ is claimed to be an excellent sensitizer and is well known to enhance the luminescent intensity for YVO₄:Eu³⁺ composites. Also, Bi³⁺ broadens the excitation spectrum of the compound.^[100,101] YVO₄:Eu³⁺, Bi³⁺, layered material has been reported in organic solar cells (OSCs) for UV protection and spectral conversion.^[101] The doping of YVO₄:Eu³⁺, Bi³⁺ as a DC material into the TiO₂ mesoporous layer has been reported for increasing the PSCs' performance and stability by Jin et al.^[102] The doping of YVO₄:Eu³⁺, Bi³⁺ in the TiO₂ layer enhances the PCE of the device from 16.7 up to 17.9%, with better stability under UV irradiation. The c-TiO₂ layer is coated on a transparent FTO electrode followed by TiO₂:YVO₄:Eu³⁺, Bi³⁺ composite paste. CH₃NH₃PbI₃ perovskite AL was then spin coated, followed by a spin-coated spiro-OMeTAD layer and a thermally evaporated Au electrode, as shown in **Figure 4a**. In an

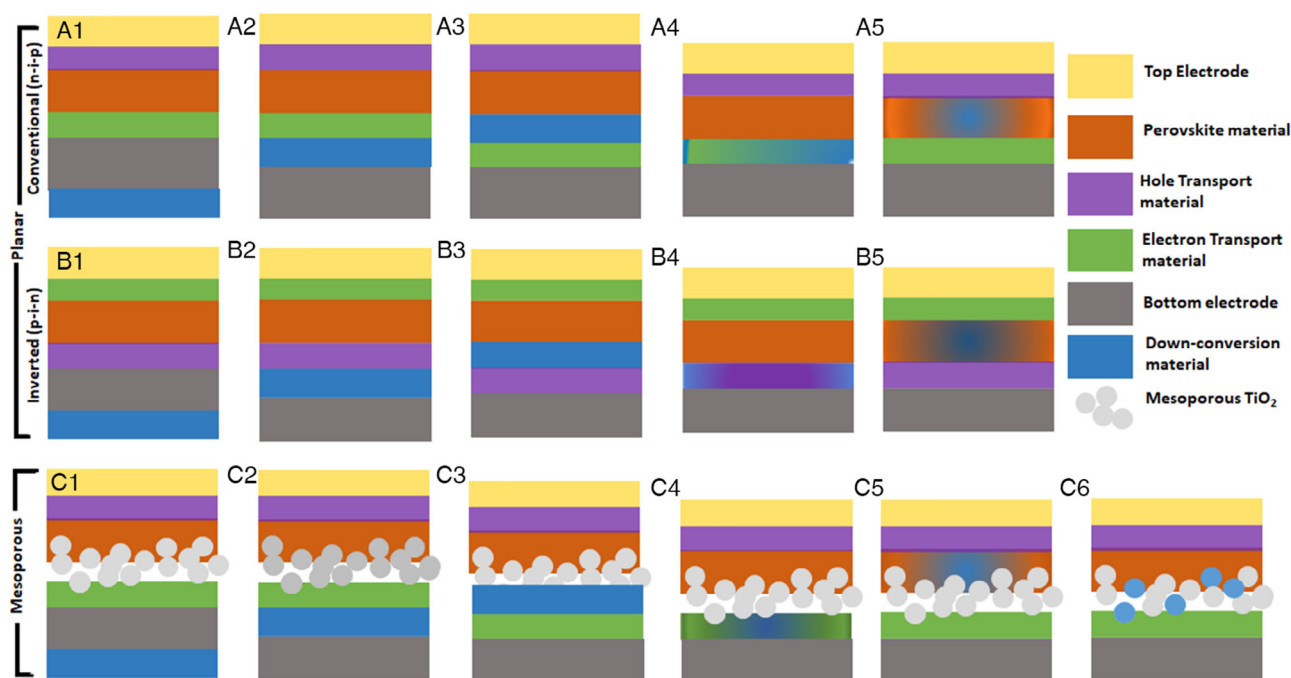


Figure 3. Structure of PSCs: (A1-5) conventional (n-i-p), (B1-5) inverted (p-i-n) junction, and (C1-6) conventional mesoporous structure.

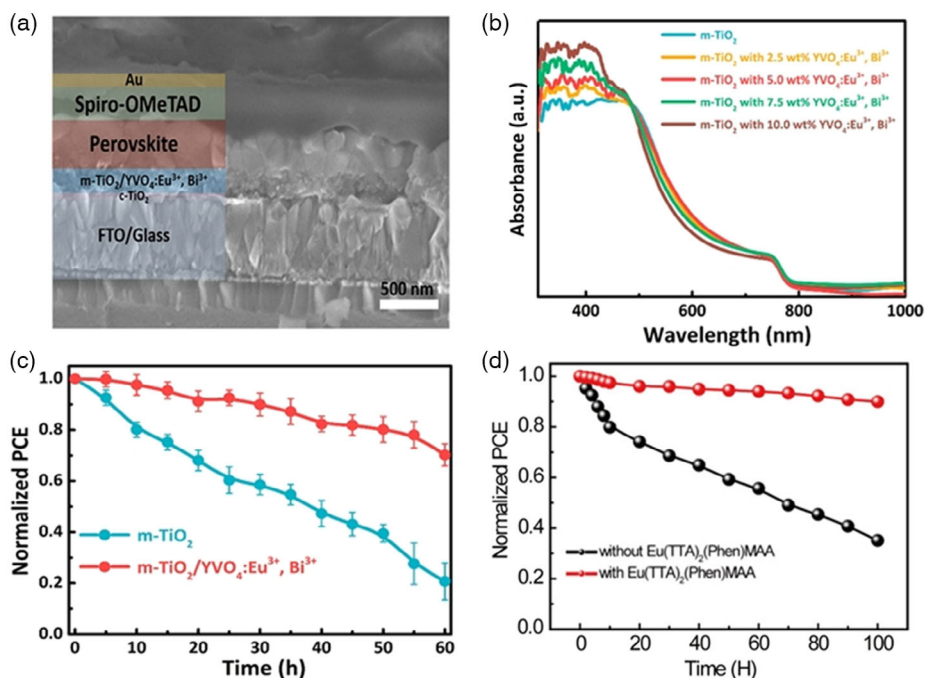


Figure 4. a) Geometry and the cross-sectional view of the $m\text{-TiO}_2/\text{YVO}_4:\text{Eu}^{3+}, \text{Bi}^{3+}$ CTL-based devices, b) UV-vis absorption property of perovskite coated on $\text{TiO}_2:\text{YVO}_4:\text{Eu}^{3+}, \text{Bi}^{3+}$ layer, and c) normalized device stability of TiO_2 and $\text{TiO}_2:\text{YVO}_4:\text{Eu}^{3+}, \text{Bi}^{3+}$ -based PSC devices. Reproduced with permission.^[102] Copyright 2018, American Chemical Society. d) Stability graph of ETMP-modified PSCs and control device under UV light (365 nm) irradiation for 100 h. Reproduced with permission.^[105] Copyright 2019, American Chemical Society.

absorption plot of pristine TiO_2 and $\text{TiO}_2:\text{YVO}_4:\text{Eu}^{3+}, \text{Bi}^{3+}$ (Figure 4b), the peak intensity rose within the 300–400 nm region as the percentage of $\text{YVO}_4:\text{Eu}^{3+}, \text{Bi}^{3+}$ increases. The measured higher absorbance toward the UV region revealed that more UV light could be used for spectral conversion. As expected, the excitation spectrum of $\text{YVO}_4:\text{Eu}^{3+}$ broadens after adding Bi^{3+} , which increases the overall UV region being converted into visible. In addition, it showed excellent UV degradation resistance due to the high absorption coefficient in the UV region and YVO_4 transfers the absorbed energy to Eu^{3+} emitting a red emission peak. The improved photovoltaic performance is evidence of enhanced cell parameters after adding $\text{YVO}_4:\text{Eu}^{3+}, \text{Bi}^{3+}$ into the TiO_2 layer. The $\text{TiO}_2:\text{YVO}_4:\text{Eu}^{3+}, \text{Bi}^{3+}$ (5%)-based devices have performance parameters of J_{sc} , open-circuit voltage (V_{oc}), and fill factor (FF) of 21.73 mA cm^{-2} , 1.10 V , and 74.9% , respectively. These contribute to a PCE of 17.9% and are significant enhancements from the TiO_2 -based control device ($J_{sc} \approx 20.62 \text{ mA cm}^{-2}$, $V_{oc} \approx 1.07 \text{ V}$, $\text{FF} \approx 73.8\%$, and $\text{PCE} \approx 16.3\%$). The device parameters are summarized in **Table 1**. The impact on device stability is shown in Figure 4c. The TiO_2 -based device holds only 20% of its initial PCE after 60 h under UV irradiation (365 nm , 25 mW cm^{-2}), whereas, under the same testing condition, $\text{YVO}_4:\text{Eu}^{3+}, \text{Bi}^{3+}$ -based device holds up to 70% of the initial PCE.

SiAlON:Eu²⁺: The phosphor particles and glass matrix, also known as phosphor-in glass (PiG), are reported as DC materials to improve PSCs' device stability under UV irradiation. The thermal conductive property of the glass matrix helps phosphor remain isolated in a harsh environment. The PiG photoluminescence properties can be modified by changing the phosphor ratio

in the glass matrix. The PiG includes $\text{SiAlON}:\text{Eu}^{2+}$ and $\text{Lu}_3\text{Al}_5\text{O}_{12}:\text{Ce}^{3+}$ as phosphors that exhibit orange and green emissions, respectively. In commercial applications such as LEDs, PiG has already been implemented and works as a dual-function DC material and encapsulation.^[103] The PiG thin films have also been proposed as suitable materials for protecting PSCs from UV radiation. Recently, Roh et al.^[104] reported the commercially available PiG thin film as DC layer for PSCs. In the study, the PiG layer was attached to the front side of the PSC device while measuring the device performance under UV (78 mW cm^{-2} , 365 nm) irradiation. Here, the PiG layer-attached devices show better UV light protection and can hold PCE up to four times than the control device, after 100 h-long UV irradiation.

Eu(TTA)₂(Phen)MAA: $\text{Eu}(\text{TTA})_2(\text{Phen})\text{MAA}$ (ETPM) possesses excitation in the UV region and re-emits the photons in the visible region due to its specific $4f$ electronic structure. This feature can boost the photogenerated current in the PSCs and protect it from UV irradiation. Bi et al.^[105] applied ETMP as an interfacial modifier between $m\text{-TiO}_2$ and perovskite layer in the conventional mesoporous PSCs. The ETMP has an absorption peak in the UV region. The ETMP-modified device exhibited a significant improvement in the PCE from 17.00 to 19.07% and played a key role in decreasing the UV-induced degradation, thereby enhancing the photostability under solar irradiation. Specifically, ETMP-modified devices maintained 86% and 90% of their initial PCE (Figure 4d) and after continuous light soaking under sunlight and UV light (365 nm) for 100 h, respectively. Li et al.^[106] also implemented ETMP as a DC material with the $\text{Yb}^{3+}, \text{Er}^{3+}/\text{Tm}^{3+}$ -doped NaYF_4 -based UC layer in PSC devices.

Table 1. A summary of photovoltaic performance of the selected lanthanide DC materials-based PSC devices.

Device structure	DC materials	Active layers [AL]	Absorption/ excitation wavelength [nm]	Photoemission peak/band [nm]	J_{sc} [mAcm ⁻²]	V_{oc} [V]	FF [%]	PCE [%]	Increment in PCE [%]	References
DC/FTO/c-TiO ₂ /AL/HTL/Au	Control	CH ₃ NH ₃ PbI ₃	200–350 nm	≈614 nm	16.53	0.83	54.0	7.42		[99]
	YVO ₄ :Eu ³⁺				17.77	0.83	53.5	7.93	6.6	
FTO/c-TiO ₂ /TiO ₂ :DC/AL/ spiro-OmeTAD/Au	Control	CH ₃ NH ₃ PbI ₃	250–380 nm	≈621 nm	20.63	1.07	73.8	16.30		[102]
	5% YVO ₄ :Eu ³⁺ , Bi ³⁺				21.73	1.10	74.9	19.70	18.8	
	10% YVO ₄ :Eu ³⁺ , Bi ³⁺				20.02	1.07	72.8	15.60		
FTO/c-TiO ₂ /DC/AL/spiro- OMeTAD/Au	Control	(CsFAMA)Pb(BrI) ₃	260–380 nm	≈615 nm	21.80	1.04	73.40	16.60		[21]
	Sr ₂ CeO ₄ :Eu ³⁺				23.70	1.06	75.53	18.95	13.2	
DC/FTO/TiO ₂ /AL/spiro- OMeTAD/Au	Control	(CsFAMA)Pb(BrI) ₃	300–400 nm	≈615 nm	20.65	1.10	74.70	16.99		[120]
	NaYF ₄ :Eu ³⁺				23.06	1.12	76.5	19.89	15.7	
FTO/c-TiO ₂ /TiO ₂ :DC/ ZrO ₂ /AL/Carbon	Control	(5-AVA) (MA)PbI ₃	240–400 nm	550–720	22.09	0.88	64.5	11.42		[130]
	TiO ₂ :EuW ₁₀ (5%)				23.46	0.88	72.4	14.60	24.4	
	TiO ₂ :EuW ₁₀ (10%)				21.43	0.89	65.1	11.73	2.6	
FTO/c-TiO ₂ /m-TiO ₂ :DC/ AL/ spiro-OMeTAD/Au	Control	CH ₃ NH ₃ PbI ₃	380–500 nm	≈613 nm	20.98	0.93	57.0	10.67		[115]
	AZO-8				23.68	0.94	62.0	13.80	25.58	
	AZO-10				22.06	0.93	58.0	11.90	10.89	
FTO/C-TiO ₂ /DC/AL/ spiro-OMeTAD/Au	Control	(CsFAMA)Pb(BrI) ₃	300–380 nm	450–620	21.22	1.02	71.1	15.4		[111]
	SCOS				23.65	1.05	72.4	17.9	15.1	

It was the first attempt in which both DC and UC layers were applied together and helped to convert UV and NIR incident photons into visible light. These layers also provided the broad absorption spectra for PSCs. The stability under 365 nm UV light irradiation revealed that DC-coated devices retain up to 94% of their initial PCE, whereas, the control device only retains 54%. The device with UC + DC layers possesses stability up to 500 h. These results clearly show the advantages of effective ETPM layers in improving device protection by conversion of harmful UV light to visible, leading to enhanced photostability.^[107] It is a significant advancement in getting long-term stability under UV irradiation.

CeO₂:Eu³⁺: Europium is another well-reported activator that is popular for imparting bright red luminescence in different host materials such as Y₂O₃, NaGdF₄, SrCeO₄, and CeO₂, for photovoltaic applications. The concept of applying CeO₂:Eu³⁺ as a DC material for enhancing the photovoltaic performance and stability under light illumination of PSCs has been incorporated by Chen et al.^[108] The energy transits from CeO₂ to Eu³⁺ ions and shows good luminescent properties. This could be used to improve PSCs' efficiency.^[109] The hydrothermal method has been used for synthesizing CeO₂:Eu³⁺ nanocrystals using trisodium phosphate dodecahydrate with sodium hydroxide (solution A) and cerium (III) nitrate hexahydrate with europium (III) nitrate pentahydrate (solution B) at different molar ratios. Solutions A and B were mixed, poured into an autoclave, and then were heated for different time periods. The emission spectra revealed the effect of nanocrystals as dopants in TiO₂ material. The CeO₂:Eu³⁺ nanocrystal-doped TiO₂ material showed highly intensive emission spectra at 590 and 607 nm wavelength,

whereas, undoped TiO₂ has no emissions. The devices were prepared from the photoactive layer using a blend of CH₃NH₃I and PbI₂(MAPbI₃) in γ -butyrolactone (GBL) and dimethyl sulfoxide (DMSO) mixed solvent. The TiO₂/CeO₂:Eu³⁺ composite layer sandwiched between TiO₂ and the photoactive layer played an important role in spectral conversion. The devices were tested under AM 1.5G solar light illumination, and the parameters are summarized in Table 1. The CeO₂:Eu³⁺ nanocrystals-based PSCs have shown improvement in J_{sc} , from 19.2 (bare TiO₂) to 20.5 (TiO₂ + CeO₂:Eu³⁺) mA cm⁻². The PCE also enhanced from 10.1 to 10.8%, and it has shown up to 6.9% improvement. The CeO₂:Eu³⁺ nanocrystal-embedded devices have a positive impact on device stability under UV illumination. The stability measurements were done under UV lamp illumination (365 nm, 184 mW cm⁻²) for different time periods without sealing the devices. The PCE of CeO₂:Eu³⁺-based devices after 50 minutes of UV illumination was maintained at 68%, whereas the control device PCE decreased to 40% of its initial value. The TiO₂ films activated the trap surface and perovskite material decomposition started under UV irradiation. These reasons were suggested as the cause of declining cell performance under continuous UV illumination.^[25]

Sr₂CeCO₄:Eu³⁺: CeCO₄:Eu³⁺ nanophosphors were added into PSCs and were discussed in a previous section. In this, strontium (Sr) was added into CeCO₄:Eu³⁺, resulting in the formation of Sr₂CeCO₄:Eu³⁺ (SCOE) as a DC, as reported by Rehman et al.^[21] This inclusion results in an improvement of the photovoltaic performance and measured device stability. The comparative device studies showed that the SCOE-coated PSCs attained high current density, PCE, and stability. The prepared SCOE

material was coated in between the c-TiO₂ ETL and triplet-cation ((CsFAMA)Pb(BrI)₃) perovskite layer followed by spiro-OMeTAD hole transport layer (HTL) layer and Au top electrode. The control device had a measured PCE of 16.60% which is lower than the SCOE-based PCE of 18.95%. The main improvement was observed in J_{sc} , which was enhanced from 21.80 to 23.70 mA cm⁻². It was claimed that the spectral conversion and modification of TiO₂/perovskite interface by SCOE was the reason behind the improvement in device parameters. The SCOE nanophosphors absorb UV light and convert it into visible, which in turn can be easily absorbed by the photoactive layer, leading to improvement in the J_{sc} of PSCs. The introduction of m-TiO₂ provides a large interfacial contact area with the perovskite layer in the PSCs and helps in the dissociation, transport, and collection of photogenerated electrons. The deposition of the SCOE layer on c-TiO₂ reduces the charge carrier recombination and improves the electron collection by preventing reverse electrode transfer from TiO₂ to the perovskite layer. This improvement in electron collection and reduction in recombination shows significant increases in the FF and V_{oc} values.^[110] Under continuous UV light (365 nm) for 70 h, the SCOE-based cell retains 80% of the PCE of its initial PCE value. In addition, the SCOE layer protects the perovskite layer from pinhole-induced recombination and UV-induced degradation. This results in the observed stable FF of SCOE-based PSCs.^[111] However, the control device shows more FF degradation. However, the device stability analysis was reported in an environment with RH of 25–30% and at 20–25 °C. The SCOE-based device retained 72% of its initial PCE after 75 days, whereas the control device lost more than 55% of its initial PCE.

ZnGa₂O₄:Eu³⁺: Zinc gallium oxide (ZnGa₂O₄) (ZGO) is an oxide phosphor that has an application in the fabrication of electronic displays.^[112] On top of this, its chemical and thermal stability are an added advantage for various other luminescent applications.^[113] The main feature of this compound is that emission occurs after the incidence of UV light, and the self-activated centers are attributed to the emission (≈525 nm), which corresponds to the GaO₆ structural unit in the ZnGa₂O₄ lattice.^[114] The ZnGa₂O₄:Eu³⁺ nanophosphor was reported by Hou et al.^[115] as a spectral converter for PSCs' application that helped in enhancing device performances as well as stability. The device geometry is shown in Figure 5a, in which the c-TiO₂ film was coated on the FTO, followed by a coating of m-TiO₂:AZO slurry, which was labeled as ZGO-6, ZGO-8, and ZGO-10 as per the dispersed amounts of 6, 8, and 10 mg mL⁻¹ AZO in the TiO₂ paste. The absorption between 380 and 500 nm wavelength became stronger as ZGO content rose. The effect on device performance is shown in Figure 5b, in which the incident photon-to-current conversion efficiency (IPCE) curve of the ZGO-8 device was inserted into the J - V characteristics. It is noticed that a lower PCE of 10.67% was reported for the control device compared with a PCE of ≈13.80% for the ZGO-8 device. This improvement corresponds to an improvement in J_{sc} from 20.12 to 23.68 mA cm⁻². The increasing IPCE between 380 and 490 nm wavelength for ZGO-8 device should be attributed to the ZnGa₂O₄:Eu³⁺ nanophosphor. The results were measured after putting the device in an environment with RH of 40–45% and a temperature of 21–23 °C in the dark. The graph is mentioned in Figure 5c. The control and ZGO-8 devices maintain up to 70%

and 66% of their initial PCE, respectively, over 9 days. The incorporation of ZGO nanophosphors helped to improve the PCE but fell short in improving device stability.

NaEuF₄: The fluoride host-doped lanthanide ions have emerged as potential candidates for optical applications as their improved luminescent properties show significant potential in solid-state lighting, bio-medical therapy, solar cells, etc.^[116,117] Ran et al.^[118] introduced NaEuF₄ nanoparticles (NPs) synthesized using a hydrothermal method. The NaEuF₄ NPs showed excitation and emission between 360–464 nm and 590–690 nm wavelength, respectively. The NaEuF₄ NPs were introduced into the m-TiO₂ and coated between c-TiO₂ and perovskite layer. It shows an improvement in the PSC device performance as well as stability. Device performance was tested for different concentrations (4, 6, 8, 10, and 12 mg mL⁻¹) of NaEuF₄ NPs after adding them into TiO₂ and the optimized results were observed for a concentration of 6 mg mL⁻¹. For the control device, the PCE was 13.03%, whereas, with the addition of NPs, the PCE of 14.51% was obtained. The major changes were observed in J_{sc} which increased from 21.76 to 22.54 mA cm⁻² and the FF, which increased from 59.29% to 63.11%. The NaEuF₄ nanoparticles' dispersions into m-TiO₂ were relatively uniform and it formed favorable morphology. It is related to the improvement in the devices' FF and J_{sc} . However, excess NaEuF₄ nanoparticles incorporation into m-TiO₂ reduces the mesoporous layer space and leads to a decrease in the adhesion of the perovskite film and cause reduction in device performance.

C₂₄H₁₆N₂:Eu: Jiang et al.^[119] introduced the Eu complex prepared from the organic molecule, 4,7-diphenyl-1,10-phenanthroline and europium (III) nitrate hexahydrate, and added it into polyvinylpyrrolidone (PVP) at different weight (0.5–1.5 wt%) concentrations. It was applied as a DC layer in PSCs and spin coated on the front side of the FTO substrate (Figure 5d). There was no absorption in pure PVP, and the layer showed high transparency in the UV-vis region. The absorption peaks showed shifting toward lower energy as the Eu complex contents increased. The photoemission region also showed an increase in the peak intensity with increasing Eu complex content in the PVP. The device structure consists of a CH₃NH₃PbI₃ perovskite layer formed by a two-step deposition method and is coated between m-TiO₂ and spiro-MeOTAD film. The effect of the Eu complex on device performance is clearly visible from the IPCE (Figure 5e) curve. In the UV region, the variation in IPCE (%) is caused by Eu complex and this IPCE enhancement is beneficial for improving the J_{IPCE} , from 16.28 to 16.76 mA cm⁻²). The Eu complex converts UV to visible light and helps to reduce the degradation caused by the UV region and therefore, improve the device stability when compared with the control devices. Eu complex cells have shown better photocurrent behavior and after 2 h under UV illumination its J_{sc} value decreases by 3%, whereas J_{sc} was reduced by up to 90% of the control devices. This clearly shows the device protection from UV light. Figure 5f shows the device PCE versus time under UV illumination for control and Eu complex devices.

NaYF₄:Eu³⁺: The europium-doped sodium (Na) yttrium (Y) fluoride (F) (NaYF₄:Eu³⁺) nanocrystals, reported by Jia et al.,^[120] absorb high-energy photons and convert them into a beneficial spectrum for enhancing PSCs' performance. These nanocrystals were deposited on the front side of the FTO substrate. The four

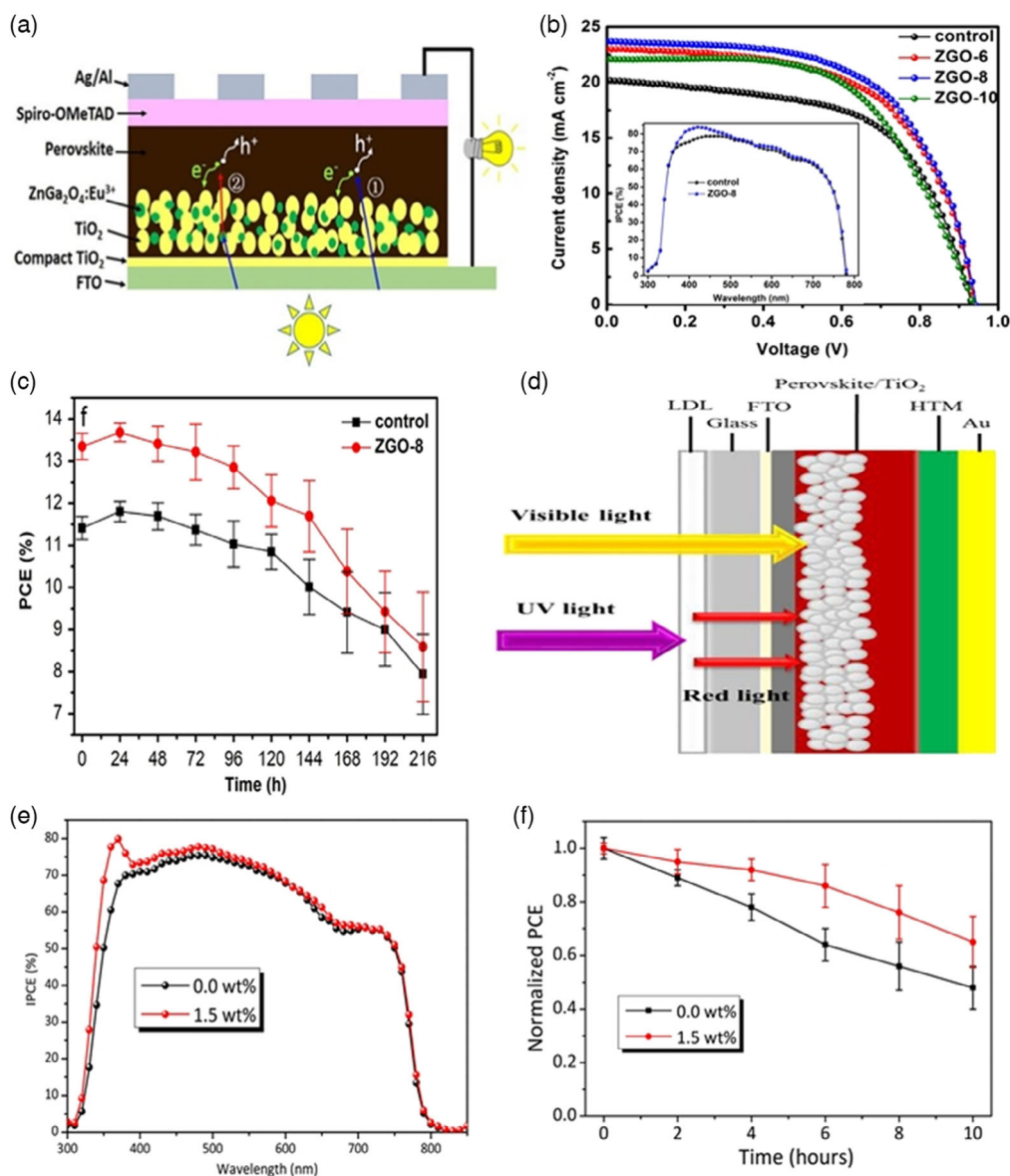


Figure 5. a) Reported device geometry of TiO_2 (control) and $\text{TiO}_2:\text{ZnGa}_2\text{O}_4:\text{Eu}^{3+}$ (AZO-6, 8, 10) with $\text{CH}_3\text{NH}_3\text{PbI}_3$ -based device, b) J - V plots (inset: IPCE curve), and c) stability plot of the control and DC material-based device, measured PCE versus time. Reproduced with permission.^[115] Copyright 2016, Elsevier B.V. d) The device structure of Eu complex coated at the front side of FTO substrate. e) IPCE curve of the device with and without Eu complex luminescent layer. f) Stability of control and 1.5 wt%-doped Eu in PVP device. Reproduced with permission.^[119] Copyright 2017, American Chemical Society.

different doping molarity (2%, 4%, 6%, and 8%) ratios of Eu^{3+} were studied and were named as $\text{NaYF}_4:\text{Eu}^{3+}\text{-}2\%$, $\text{NaYF}_4:\text{Eu}^{3+}\text{-}4\%$, $\text{NaYF}_4:\text{Eu}^{3+}\text{-}6\%$, and $\text{NaYF}_4:\text{Eu}^{3+}\text{-}8\%$, respectively. For PSCs, the triple-cation $\text{Cs}_{0.05}(\text{MA}_{0.17}\text{FA}_{0.83})_{0.05}\text{-Pb}(\text{I}_{0.83}\text{Br}_{0.17})_3$ perovskite layer was coated above the TiO_2 ETL, followed by a spiro-OMeTAD HTL and Au top electrode. The transmittance of $\text{NaYF}_4:\text{Eu}^{3+}/\text{FTO}$ was higher in the visible region as compared with UV, which is evidence of absorbing a certain amount of UV light. Moreover, $\text{NaYF}_4:\text{Eu}^{3+}$ has photoemission between 500 and 750 nm wavelength and showed an increase in intensity with an increase in Eu contents. It showed that the device performance for 2%, 4%, 6%, and 8% molarity ratios is better than

the control devices. Here, PSCs-6% obtained a PCE of $\approx 20.17\%$, which is an improvement over control device performance with a measured PCE of $\approx 19.65\%$. In addition, the PSCs-6% device exhibited a small amount of hysteresis under the reverse (PCE: $\approx 19.89\%$) and the forward scan (PCE: $\approx 18.74\%$). Another important effect was reported under UV irradiation. The PCE value of control PSCs degraded at a faster rate under continuous irradiation for 10 h as compared with PSC-6% device. The results undoubtedly show that the $\text{NaYF}_4:\text{Eu}^{3+}$ nanophosphors can reduce UV-induced degradation and can impact the device by offering improved performance and stability.

$Au@Y_2O_3:Eu^{3+}$: Yttrium oxide (Y_2O_3) exhibits outstanding optical and electrical properties such as a larger bandgap, a high refractive index, superior electrical breakdown strength, etc.^[121,122] It is one of the most attractive RE oxides and has been applied as a phosphor film for cathode ray tube (CRT) displays. It is also used as an UC material for cellular imaging.^[123] $Y_2O_3:Eu^{3+}$ core-shell and nanoparticle material structures were studied, which are popularly known as red phosphor. By having a good QE, it is used in industry to fabricate flat panel displays.^[124] The core-shell structures of gold (Au) and silver (Ag) have attracted much attention because they enhance the physical and chemical properties of its compounds. The Au-doped $Y_2O_3:Eu^{3+}$ is a well-reported phosphor material which might have potential applications in optical devices.^[125] Kim et al.^[126] introduced $Au@Y_2O_3:Eu^{3+}$ as a DC layer in PSCs. Initially, $Y_2O_3:Eu^{3+}$ phosphor monolayer has shown more than 80% photoluminescence quantum yield.^[127] Recently, the Au nanoparticle layer attached with $Y_2O_3:Eu^{3+}$ amplified the converted visible light up to 170%. The $Y_2O_3:Eu^{3+}$ nanocrystals are coated on top of the Au film and then annealed at 450 °C to form strong adherence with the substrate. The DC layer is coated on the front side of the FTO substrate (Figure 6a). The measured optical properties of the Au nanoparticles and phosphor revealed that the phosphor particle layer has a peak absorption spectrum (Figure 6b) at 290 nm. However, the Au nanoparticle-localized surface plasmon absorption peak was

spotted at 520 nm. Notably, the $Au@Y_2O_3:Eu^{3+}$ thin-film photoemission intensity improved by 70% compared with the pristine phosphor material. This light amplification directly influences the PSCs' efficiency, and its dual-function nature protects the perovskite layer from UV light degradation. The DC layer contributed to enhancing the PCE up to 16.1% compared with the control device. The dual functionality of the layer influences the photocurrent values of the $Au@Y_2O_3:Eu^{3+}$ -based devices. J_{sc} was 21.5 mA cm⁻² for the dual-function layer-attached PSCs compared with 20.7 mA cm⁻² of control device. This confirms that UV light is converted into visible and helps in enhancing the photogenerated current. Figure 6c shows the normalized plot of photogenerated current density versus time under UV irradiation and shows that the DC protected the PSCs from harmful UV-induced degradation.

$Na_9[EuW_{10}O_{36}]$: Polyoxometalates (POMs) are the combinations of oxygen and early transition metals (e.g., M = Mo, Ta, W, Nb, V) or kinds of molecular metal-oxocluster compounds.^[128,129] POMs can be prepared using lanthanides and are formed via strong coordination bonds. These possess advantages such as good luminescent properties, water solubility, high stability, and low cost. The europium-containing POM $Na_9[EuW_{10}O_{36}]$ (EuW_{10}) material, reported by Tao et al.,^[130] was introduced as a DC layer and coated with TiO_2 layer for improving the performance of printable PSCs by converting high-energy to low-energy photons. The reported EuW_{10} -based

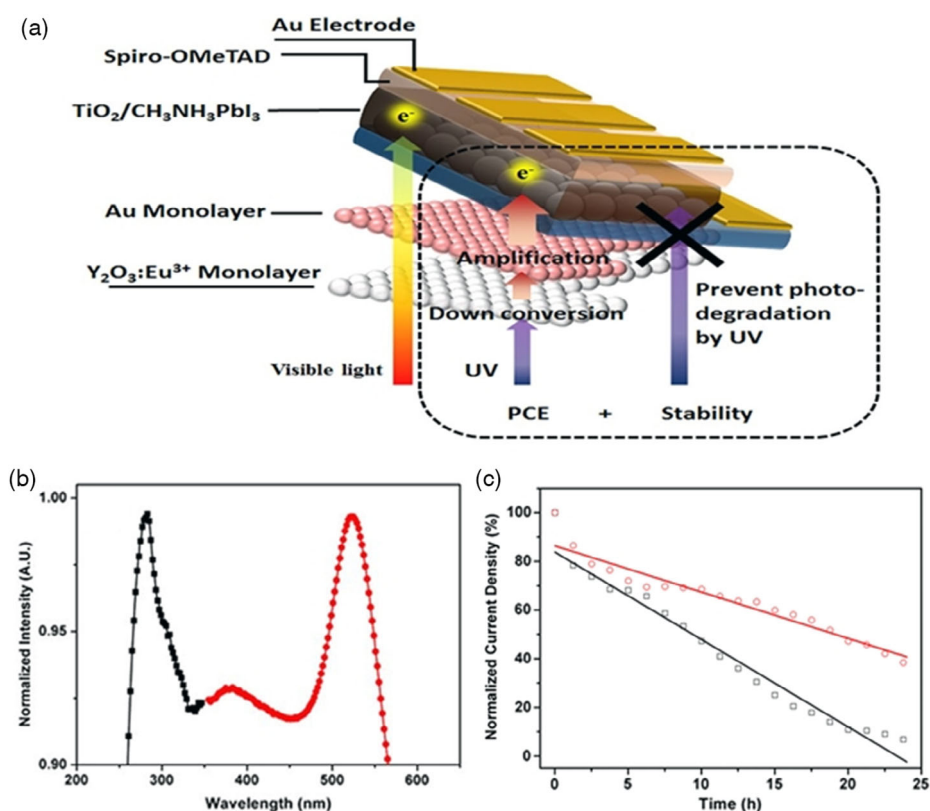


Figure 6. a) The device geometry with working mechanism of dual-function film, b) absorption (black color) and photoemission (red color) spectra of Au NPs and phosphor particle layers, and c) long-term stability measurement of control (black) and $Au@Y_2O_3:Eu^{3+}$ (red)-based PSCs. Reproduced under the terms of the CC-BY license (CC BY 4.0).^[126] Copyright 2017, the Authors. Published by Springer Nature.

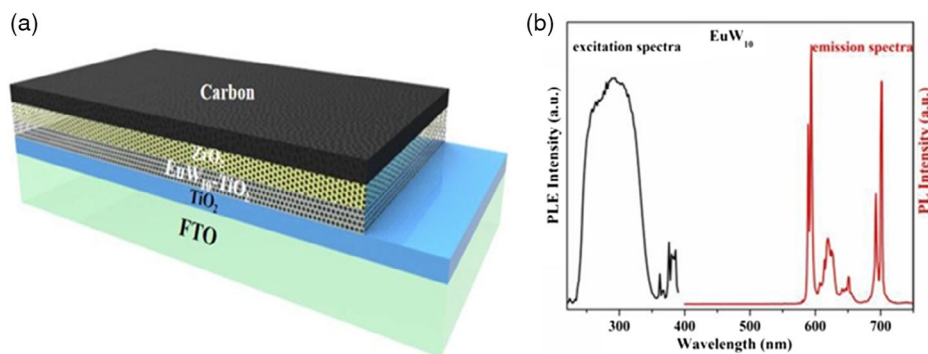


Figure 7. a) Geometry of device structure and b) emission and excitation spectra of EuW_{10} powder. Reproduced with permission.^[130] Copyright 2020, Elsevier B.V.

PSC device exhibited long-term stability as compared with the control devices. The emission (ranging from 550 to 720 nm) and excitation (covering the range from 240 to 400 nm) of EuW_{10} are shown in **Figure 7b**. These spectra demonstrated the conversion of UV photons to visible using EuW_{10} powder. The PSCs were prepared using screen printing and the device geometry is mentioned in **Figure 7a**. The control device exhibits a PCE of 11.1%, with J_{sc} of 20.09 mA cm^{-2} and for EuW_{10} -based PSCs, the PCE was 14.36%, which improved due to an increase in the J_{sc} of $\approx 23.46 \text{ mA cm}^{-2}$, for 5% EuW_{10} contents. After increasing EuW_{10} contents to 10%, the device performance begins to decline. Increasing the contents of EuW_{10} may increase the cell resistance and result in a reduction of the J_{sc} and FF. In addition, the EuW_{10} - TiO_2 based device showed slightly higher stability than the control devices. Overall, EuW_{10} -based layers help to enhance the device performance by 25% and improve the device stability.

3.1.2. Samarium (Sm)-Based DC Materials

P_2O_5 - Li_2O - ZnO - Sm_2O_3 - CeO_2 (PZLSC) Glass-Ceramic: The doping of Sm and Ce ions into the flexible glass system (P_2O_5 - ZnO - Li_2O (PZL)), which is defined as P_2O_5 - Li_2O - ZnO - Sm_2O_3 - CeO_2 glass-ceramic waveguide (GCW), has also been applied to PSCs as a DC layer.^[131] The GCW helped to enhance the performance and stability of the devices. Moreover, the PZL material has high transparency, good solubility for Sm and Ce, and low-melting-temperature properties that make it a suitable host for making GCW. The GCW: Sm^{3+} sample has excitation in the range of long-wavelength UV (LWUV) 300–500 nm and emission at $\approx 597 \text{ nm}$, indicating its application as a DC material. However, Ce^{3+} was codoped as a sensitizer in the GCW Sm^{3+} system, which results in Sm^{3+} emission intensity enhancement. The excitation intensity also improved for GCW: Sm^{3+} - Ce^{3+} system than in the GCW: Sm^{3+} system. Moreover, Ce^{3+} also has strong absorption in LWUV and efficiently transfers energy from Ce^{3+} to Sm^{3+} , which is promising in reducing UV-based photodegradation in PSCs. The GCW: Sm^{3+} - Ce^{3+} compound was prepared via the high-temperature melt-quenching method and has been coated on the front of FTO glass substrates. The PSCs device with DC showed more than 9% enhancement in J_{sc} and PCE. Tin oxide (SnO_2) is a popular ETL in PSCs and helped to deliver PCEs up to 21%.^[132]

It is also compatible with flexible devices.^[133] Recently, Singh et al.^[134] demonstrated Sm^{3+} -doped SnO_2 nanoparticles and investigated different annealing temperatures and concentrations to probe the effects on photoluminescence properties of prepared composites and its implementation as a DC material for PSC devices.

$\text{Sr}_2\text{CeO}_4:\text{Sm}^{3+}$: Cerium-strontium oxide (Sr_2CeO_4) is a perovskite structure oxide, and it is a promising blue phosphor that exhibits luminescence under excitation. It is also used in various applications such as fluorescent tubes, detection and field emission displays, etc.^[135,136] In Sr_2CeO_4 , the blue emission band at 473 nm is attributed to the $-\text{Ce}^{4+}-\text{O}^{2-}$ charge transfer and it has broad excitation in the UV region that opens up the possibility of tuning its excitation energy.^[137] Therefore, the Sr_2CeO_4 compound could act as a host for lanthanide ions. An appropriate luminescence activator such as Sm, Eu, and Gd from the lanthanide series has been widely reported for enhancing and tuning the luminescent properties of its compound.^[138] After Sr_2CeO_4 is doped with Eu and Gd, its photoluminescence (PL) emission mainly covers the 350–650 nm range.^[139] Recently, Sm-doped Sr_2CeO_4 , named as $\text{Sr}_2\text{CeO}_4:\text{Sm}^{3+}$ (SCOS), was introduced into PSCs by Rahman et al.^[111] and achieved an enhancement of the photogenerated current by up to 11.4%, and the device held 50% of its initial value of PCE after 60 h under UV light irradiation. This photogenerated current improvement is much more significant when compared with previously reported DC materials such as $\text{Y}_2\text{O}_3:\text{Eu}^{3+}$ and $\text{CeO}_2:\text{Eu}^{3+}$ and possesses higher photostability. It has an absorption spectrum that covers the range of 283–400 nm, with the peak intensity varying with respect to Sm^{3+} concentrations (0.5, 1.0, 1.5, and 2.0 wt%). Moreover, the absorption characteristics showed a rise in intensity as Sm^{3+} content was increased and reached its highest value at 1.5 wt% concentration. The PL characteristics showed SCOS emission in the visible region and has peaks at 480, 564, 608, and 647 nm wavelength that were attributed to different transitions. In the geometry of the fabricated PSCs, $(\text{CsFAMA})\text{Pb}(\text{Br})_3$ was used as a photoactive layer. The SCOS layer was sandwiched between c- TiO_2 and photoactive layers. The average PCE of SCOS-based PSC devices was 17.9%, which shows an improvement from the control device with a PCE of 15.2%. Besides the increase in PCE, the SCOS layer also protected devices from UV light, temperature, and humidity. The SCOS-based PSC device was placed under continuous irradiation under UV light

(365 nm) at room temperature and 25–30% humidity for 65 h. The control PSC device retains only 19% of its initial value after 35 h; on the other hand, the SCOS device contains 67% of its PCE. After 60 h, SCOS devices have shown great UV light stability. These devices were also kept in ambient environment without encapsulation for 60 days and showed that the SCOS-based devices retain higher device performance as compared with the control devices.

3.1.3. Lanthanide Materials Doped in TiO₂ Layer

TiO₂ nanomaterials have been extensively studied in the last two decades and their novel properties such as chemical stability, nontoxicity, and biocompatibility have shown their potential applications in optical coating, photocatalysis, antibacterial agents, and solar cells.^[140] In solar cells, TiO₂ is commonly used as an ETL in organic photovoltaics as well as PSCs.^[141] Recently, lanthanides modified with TiO₂ were reported for their use in different applications. Zeng et al.^[142] coated Eu with TiO₂, and the concentration of Eu³⁺ influences the energy transfer between Eu and TiO₂. Moreover, Nd and Sm lanthanide materials have also been incorporated into TiO₂ nanoparticles, and it was found that it exhibits more emission via the doped compounds than from direct excitation of pristine materials.^[143] Furthermore, lanthanides doped into TiO₂ compounds were used in PSCs for UV light protection and performance enhancement. Jiang et al.^[144] prepared the TiO₂:Eu³⁺ crystals via the sol-gel method and sandwiched the crystals between the c-TiO₂ and CH₃NH₃PbI₃ perovskite layer, as shown in **Figure 8a**. The devices with Eu doping in TiO₂ show an improvement in PCE from 12.22 to 15.79%, and that was up to 29.2% improvement as compared with the control device. This significant enhancement in the PCE is attributed to increases in light absorption. Moreover, Eu doping embedded in the surface sites adjacent to TiO₂ helps to suppress the recombination in TiO₂, which results in an improvement in the V_{oc}.^[145] However, at higher Eu concentrations, defects are created at the TiO₂ boundary, which cause excessive particle build-up with higher ionic radius and result in PSC performance degrading. Photoluminescence quantum efficiency (PLQE) was 9% for TiO₂:Eu³⁺ from UV light to visible (red) emission. The Eu ion doping not only improved the J_{sc} but also improved the V_{oc}, which results in overall PCE improvement. Furthermore, Eu concentration also affects the device stability, as shown in **Figure 8b**. The control device PCE decreased by up to 50% under continuous UV irradiation for 10 h. However, Eu³⁺-doped TiO₂ structure PSCs show protection under UV irradiation by preventing the degradation of the perovskite layer. Recently, Zhang et al.^[146] doped TiO₂ with Sm and Eu ions and applied it as an ETL in the PSC device via optimizing the ratio of these materials. PL quenching (**Figure 8c**) increased after introducing Sm into Eu:TiO₂. PL quenching of TiO₂ indicates that the proper introduction of lanthanide materials can improve electron collection and their transport efficiency. The photovoltaic performance of the MAPbI₃ perovskite layer-based device with pulsed laser deposition (PLD)-deposited ETL TiO₂:Sm³⁺, Eu³⁺ (0.8%, 1%) exhibits a PCE of 19.01%, which is higher than the control devices (PCE: 16.90%). The ETL layer also protects the devices from

harmful UV light irradiation. **Figure 8d** shows the control and Sm- and Eu-doped TiO₂ PSC devices tested under a UV lamp (356 nm, 23 mW cm⁻²). Chen et al.^[147] reported that Eu-doped TiO₂ materials, prepared by the chemical bath method, enables simultaneous efficiency and UV stability enhancement. This dopant (Eu) helps shift the Fermi-level energy and enhances the electron mobility of TiO₂.^[148] Besides this, the average charge carrier extraction time of the perovskite film coated on Eu³⁺:TiO₂ and TiO₂ was 23.34 and 29.93 ns, respectively, as calculated from the time-resolved photoluminescence decay (**Figure 8e**) measurement. The shorter time of the Eu ions-doped TiO₂ suggests a faster electron extraction process, which is beneficial for device performance. Different concentrations of Eu ions were doped into TiO₂, and the optimized results were obtained at 5% of Eu, where the PCE was 21.40% (J_{sc} ≈ 23.85 mA cm⁻², V_{oc} ≈ 1.13 V, and FF ≈ 0.79) and is a significant improvement than control device (PCE of 19.22%). Also, higher stability is reported under UV irradiation (365 nm, 5 mW cm⁻²) under ambient conditions up to 500 h. The Eu³⁺:TiO₂ device retains 80% (**Figure 8f**) of its initial value for 100 h and up to 70% for 500 h. In comparison, the control device remains at 50% for 100 h and then undergoes aging degradation affecting the J_{sc} and FF. This degradation is mainly due to the decomposition of the perovskite layer under UV irradiation. Cerium ions (Ce³⁺)-based nanophosphor Y₃Al₅O₁₂:Ce³⁺ (YAG:Ce³⁺) have also been introduced into m-TiO₂ and applied as a spectral modifier by Ma et al.^[149] The YG:Ce³⁺-doped TiO₂-based PSCs improve V_{oc}, FF, and J_{sc} parameters. The YAG:Ce³⁺ absorption band lies in the UV region and shows broad emission between 500 and 700 nm, which causes an improvement in the J_{sc} of YAG:Ce³⁺-based devices. However, the substitution of Ce ions at the Ti lattice side in TiO₂ probably modified the electronic energy level of the doped film, which resulted in an increase in the V_{oc}. The doping of YAG:Ce³⁺ DC materials improved the PCE up to 13.34%, which was higher than the control device PCE of ≈ 11.04%.

3.2. Nonlanthanide Materials-Based Spectral Convertors for PSCs

Besides lanthanide materials, various lanthanide-free materials have been explored for spectral conversion applications for PSCs. Such materials are cost effective, which is a major concern for PV devices.

3.2.1. Nanophosphor Materials

Sr₄Al₁₄O₂₅:Mn⁴⁺: The Sr₄Al₁₄O₂₅:Mn⁴⁺, 0.5% Mg (SAM) nanophosphor was used as a DC material in PSCs and its inclusion caused 10% rise in PCE and an improvement in the stability in SAM-based devices, as published by Cui et al.^[150] This phosphor shows red luminescence with high intensity due to Mg ions. Before coating, the DC layer was embedded in PMMA and coated on the front side of the FTO substrate. The SAM/PMMA film has a broad excitation range from 290 to 520 nm and photoemission in the visible region (red). For 380 and 470 nm excitation wavelength, it shows the PLQE of 38 and 35%, respectively. Thus, the DC layer reduced the direct absorption of UV light into the

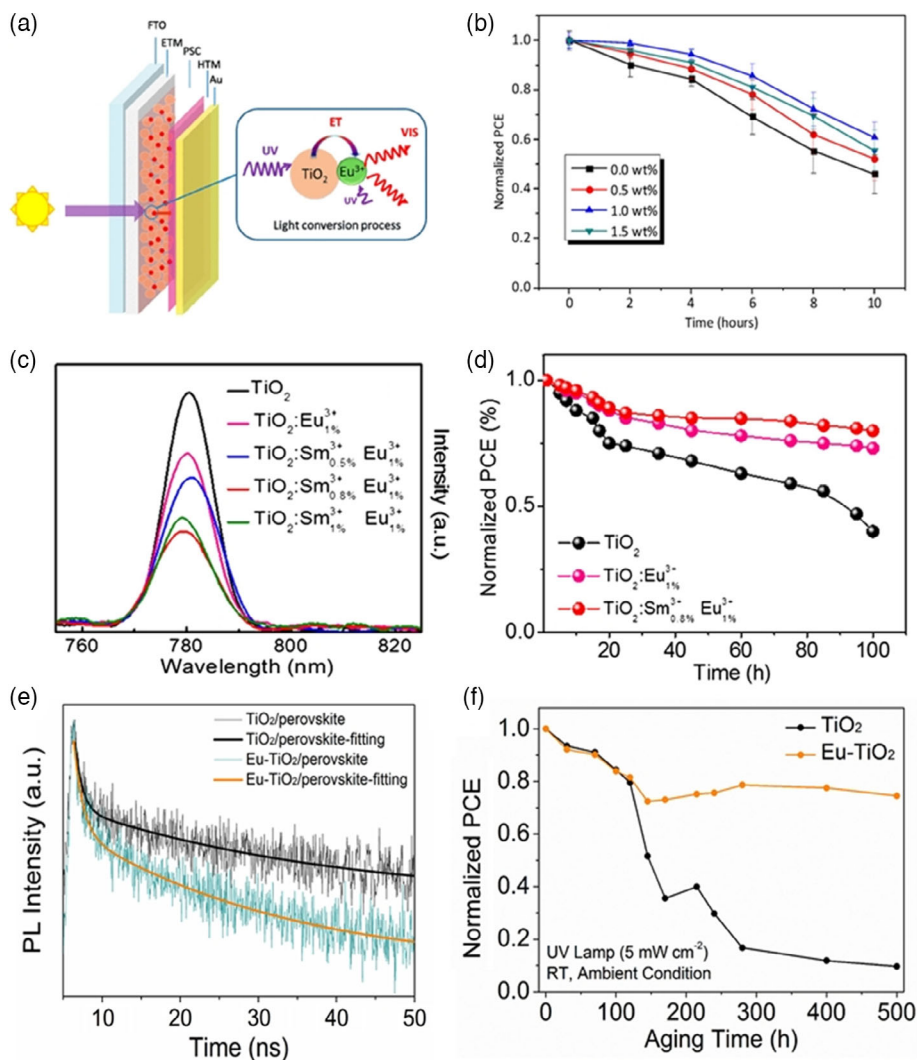


Figure 8. a) Schematic illustration of PSC device structure, explaining the mechanism of energy transfer between TiO_2 and Eu ions and b) normalized PCE stability under UV (UV – Hg-200 light source) irradiation of control and Eu ion-doped TiO_2 devices at different concentrations of Eu ions. Reproduced with permission.^[144] Copyright 2018, American Chemical Society. c) Emission quenching spectra of the perovskite layer coating at different ratios of Eu and Sm ions and d) normalized PCE stability reported under 365 nm UV light continuous irradiation up to 100 h. Reproduced with permission.^[146] Copyright 2019, Elsevier Inc. e) TRPL-fitted curve of $(\text{Cs}_{0.05}\text{FA}_{0.80}\text{MA}_{0.15})\text{Pb}(\text{I}_{0.85}\text{Br}_{0.15})_3$ perovskite layer coated on $\text{FTO}/\text{Eu}^{3+}:\text{TiO}_2$ and FTO/TiO_2 substrates. f) Normalized PCE stability of $\text{Eu}^{3+}:\text{TiO}_2$ and TiO_2 -encapsulated devices under continuous UV light irradiation for 500 h. Reproduced with permission.^[147] Copyright 2019, Elsevier Ltd.

perovskite layer and enhanced the film stability. The studies of film degradation by XRD have shown that the SAM/PMMA film provides encapsulation capability to the perovskite layer and reduces moisture-based degradation under ambient conditions. The control device gives a J_{sc} of 18.2 mAcm^{-2} and a PCE of about 12.6%. For a DC (1.2 mg ml^{-1})-based device, there is an enhancement of the J_{sc} up to 19.6 mAcm^{-2} , which contributed to delivering PCE up to 14%. This enhancement of J_{sc} has shown the advantage of incident light spectral modification.

3.2.2. QDs

$\text{CsPbCl}_3:\text{Mn}$: The QDs are 3D confined particles that exhibit excellent luminescence properties. These are a superior class

of semiconductors that are crystalline or amorphous, have 2D or 3D structures, and are prepared from periodic groups of II–VI, III–V, or IV–VI materials.^[151] Its energy levels and energy gap depend on its diameter. The adjustable energy gap of QDs allows for applications in multiple fields, including solar cells, and recently, it emerged as a DC material in PSCs.^[152] The DC layers of $\text{CsPbCl}_3:\text{Mn}$ QDs have been reported by Wang et al.^[153] and were applied on the front sides of the FTO substrate. Mn ions doped in CsPbCl_3 exhibit enhanced emission properties. The hot-injection method was used to prepare the QDs, and this technique had shown a PL quantum yield of up to 60%. **Figure 9a** illustrates the energy transfer between CsPbCl_3 and Mn QDs, where CsPbCl_3 works as a host and can be excited at 365 nm, and also exhibiting a broad emission

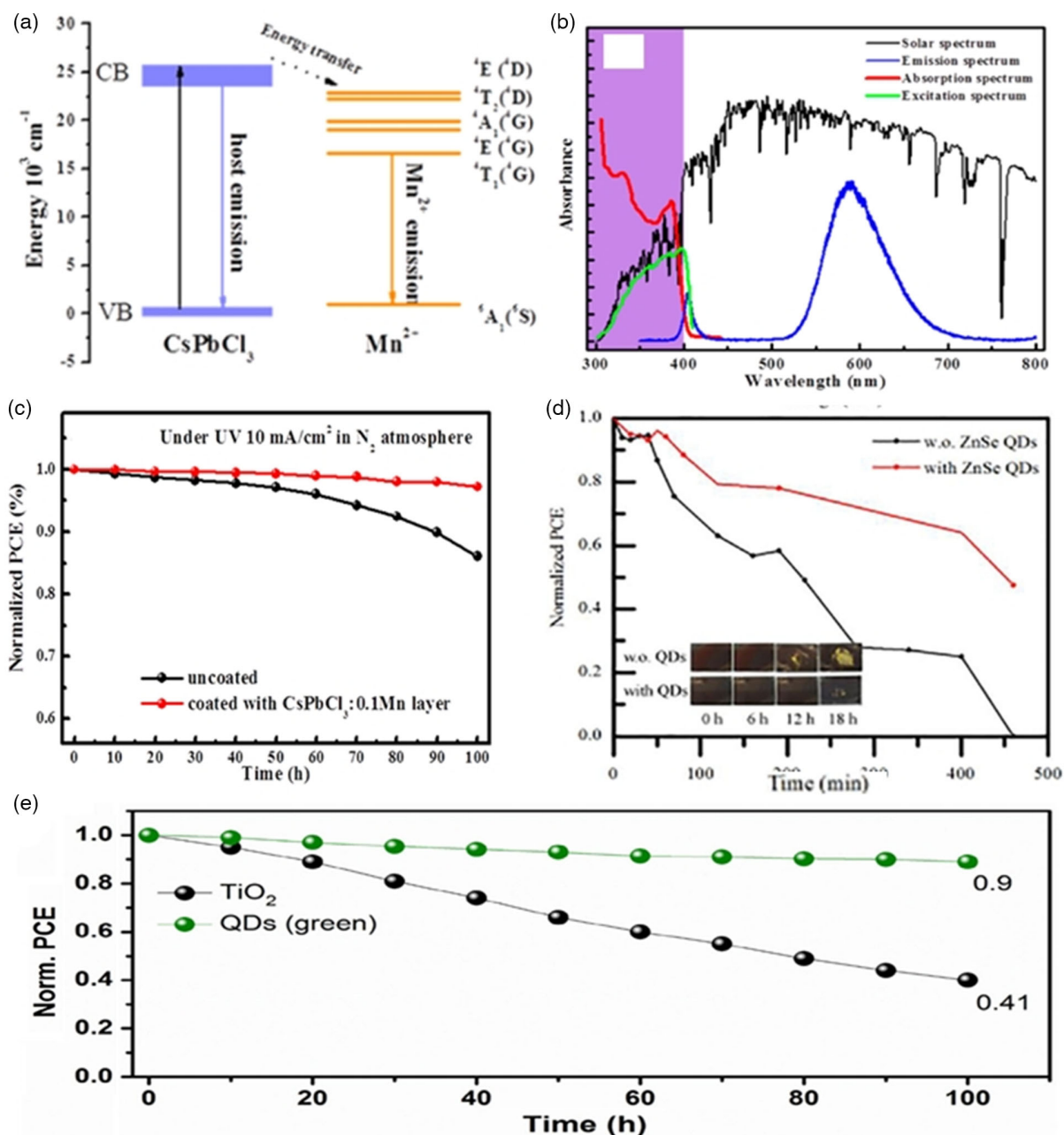


Figure 9. a) Illustration of DC mechanism in CsPbCl₃:Mn QDs, b) excitation and emission spectra of CsPbCl₃:Mn QDs, and c) normalized PCE values for control and optimized device under UV irradiation. Reproduced with permission.^[153] Copyright 2017, American Chemical Society. d) Normalized PCE reported measurement after the aging test with QDs and control device (inserted devices' pics under UV irradiation). Reproduced with permission.^[156] Copyright 2017, Science Press and Dalian Institute of Chemical Physics, Chinese Academy of Sciences. Published by Elsevier B.V. and Science Press. e) The normalized PCE of TiO₂ and QD (green) devices under UV light. Reproduced with permission.^[160] Copyright 2020, Wiley-VCH.

spectrum in the visible region. This is displayed in Figure 9b. The control device has a J_{sc} and PCE of 21.23 mAcm⁻² and 17.97%, respectively. For the QD optimized (5 mg ml⁻¹) device, the PCE of 18.57% and J_{sc} improved up to 22.03 mAcm⁻², respectively. The impact of using QDs was also observed for improving device stability under continuous UV irradiation up to 100 h, as shown in Figure 9c. The QD-coated device retained

97% of its initial PCE value compared with the control device which only retained 85%.

ZnSe: The ZnSe QDs are another promising material that can be used in solar cell applications due to its favorable optical properties.^[154,155] Recently, the ZnSe QD layer was introduced as a DC layer by Wang et al.^[156] and it was coated on the front side of the FTO substrate. The resultant device received enhanced

efficiency and stability. ZnSe is a wide-bandgap (≈ 2.7 eV) semiconductor and its QDs can efficiently absorb UV light while having emission in the visible. These QD-based devices using a $\text{CH}_3\text{NH}_3\text{PbI}_3$ perovskite layer reported a PCE improvement from 16.6 to 17.3%, and it is due to the enhancement in the incident visible light. These devices also have shown better stability under UV irradiation as compared with control devices, as shown in Figure 9d. The control device performance rapidly declined under UV exposure after 460 minutes, whereas, the device with ZnSe QDs holds 50% PCE of its initial value for the same length of time.

CdSe: Cadmium selenide (CdSe) QDs are well reported in DSSC, organic, and PSCs as an interface layer and as a doping agent into the photoactive layer, and it enhanced the PCE by suppressing charge carrier recombination.^[157,158] Recently, Tavakoli et al.^[159] introduced CdSe/CdS QDs as DC layers coated on the front side of the FTO substrate and applied in Cs/FA double A-cation composition perovskite devices. They found that under 40% RH in ambient air atmosphere, it is effective in increasing the perovskite film quality after annealing. This AL annealing and QD layer together enhanced device performance as high as 20.70% PCE from 18.4% and increased stability under UV irradiation. The control device has a J_{sc} , FF, and PCE of 22.10 mAcm^{-2} , 75%, and 18.4%, and these were enhanced up to 23.05 mAcm^{-2} , 77%, and 20.2%, respectively for the ambient-annealed device. However, for QD devices, the PCE improved from 20.08% to 20.70%. These QDs gave a PL quantum yield up to 85%. Apart from the efficiency improvement, these QDs have shown improved PSC stability under continuous illumination of light and under UV light. Tavakoli et al.^[160] reported the first incorporation of CdSe/ZnS core-shell QDs of green and red emissions as an ETL and DC dual layer. The measured PLQE was 85% for these QDs and showed how efficient it is at converting high-energy photons to low-energy photons. They concluded that green emission (520 nm) QDs are more efficient and have the best suitable band alignment with the perovskite film as

compared with red emission (640 nm). Moreover, the conduction bands of TiO_2 , QDs (green), QDs (red) are -4.2 , -4.08 , and -4.12 eV, respectively. This shows that band offset between perovskite (-3.9 eV) and green QDs is only 0.180 eV, which is comparatively lower than TiO_2 and red QDs. The replacement of TiO_2 by QDs (green) gave comparable device performance and provides better stability under UV irradiation. TiO_2 , QDs (red), and QDs (green)-based ETL devices a recorded PCE of 18.15, 15.8, and 18%, respectively. However, the impact of photon energy conversion was apparent when looking at the measured J_{sc} values from IPCE, as the QD (green) device gave a J_{IPCE} of 22.3 mAcm^{-2} , which was higher compared with the TiO_2 (21.7 mAcm^{-2}) and QD (red) (22.1 mAcm^{-2})-based devices. Apart from this, QD ETL-based devices were more stable under UV light irradiation and the stability plot is shown in Figure 9e. The QD devices maintained up to 90% PCE of its initial value after exposure to UV light for 100 h, which is significantly higher when compared with the TiO_2 (PCE $\approx 59\%$) devices (Table 2).

3.2.3. Carbon and Graphene QDs

Carbon QDs: Carbon-based materials also provide promising candidates for optoelectronic and photovoltaic devices. They offer highly tunable structures with a controlled Fermi level, tunability of optical and electrical properties, easy availability, low cost, etc. They also hold a variety of other important properties such as mechanical and chemical stability, thermal conductivity and good charge carrier mobility, etc.^[161] These carbon-based materials include graphitic carbon nitride, graphene and graphene oxide, carbon QDs and nanotubes, etc. as interlayers in solar cells.^[162,163] Ku et al.^[164] first reported the use of a carbon material in PSCs in which carbon/graphite was applied as a counter electrode for fully printable solar cells. Recently, fluorescent carbon dots (CDs) were incorporated by Jin et al.^[24] in the mesoporous TiO_2 interlayer for enhancing the photostability and

Table 2. A summary of photovoltaic performances of selected nonlanthanide DC material-based PSC devices.

Device structure	DC materials	Active layers [AL]	Absorption/excitation wavelength [nm]	Photoemission peak/band [nm]	J_{sc} [mAcm^{-2}]	V_{oc} [V]	FF [%]	PCE [%]	Increment in PCE [%]	References
DC/FTO/ TiO_2 /AL/SpiroOMeTAD/Au	Control	$\text{CH}_3\text{NH}_3\text{PbI}_3$	300–400 nm	550–700	21.23	1.105	76.6	17.97		[153]
	$\text{CsPbCl}_3\text{:Mn}$ (5 mg mL^{-1})				22.03	1.105	76.3	18.57	4.2	
DC/FTO/ TiO_2 /AL/SpiroOMeTAD/Au	Control	$\text{CH}_3\text{NH}_3\text{PbI}_3$	300–380	390–480	20.2	1.1	76.9	16.6		[156]
	ZnSe (2 mg mL^{-1})				20.3	1.1	79.9	17.3	4.1	
DC/ITO/NiO/AL/ C_{60} /BCP/Ag	Control	Mixed halides	–	580–650	23.1	1.14	76.2	20.08		[159]
	CdSe/CdS				23.6	1.14	76.8	20.70	3.0	
FTO/ TiO_2 /DC/AL/spiro-OMeTAD/Au	Control	MAIPbCl ₂	320–360	400–475	20.89	1.01	68.9	14.61		[24]
	CDs				22.64	1.01	71.6	16.40	11.5	
DC/FTO/ TiO_2 /AL/PTAA/Au	Control	CsPbI_2	200–400	520–700	18.67	1.10	75.4	15.53		[175]
	N-CQDs				19.15	1.16	75.6	16.02	3.10	
DC/FTO/ <i>c</i> - TiO_2 / <i>m</i> - TiO_2 /AL/Spiro-OMeTAD/Au	Control	Mixed halides	300–420	400–540	21.96	1.07	74	17.31		[183]
	V570				23.23	1.09	74	18.67	7.5	
FTO/DC/AL/PCBM/BCP/Ag	Control	MAPbI ₃	–	400–600	19.76	1.02	74.6	15.18		[185]
	2.5 wt% NPB				22.32	1.06	76.7	18.23	18.1	

performance of PSCs devices. As a result, the CDs could effectively improve the PCE of the device up to 16.4% as compared with the control device (PCE \approx 14.6%). This was achieved through the UV light into visible region conversion. As per the device geometry (Figure 10a), the CD layer was deposited by dipping the FTO/c-TiO₂/m-TiO₂-coated substrate into the CD solution under a dark atmosphere for different times; the film was formed between the m-TiO₂ and perovskite layer. Moreover, different concentrations (0, 0.5, 1, 2.0, 4.0 mg mL⁻¹) of CD solution were studied, and the *J*-*V* characteristics are shown in Figure 10b. The highest photovoltaic performance was achieved at 1 mg mL⁻¹ concentration and the device delivered a PCE up to 16.40%. This was higher than the control device with a PCE of 14.61%. In addition, CD-based devices retained 70% of its initial PCE after continuous illumination up to 12 h in ambient condition without encapsulation. The normalized PCE is shown in Figure 10c. In the same period, the reference devices only retained 20% of its initial PCE. The photostability improvement of PSCs with CDs is attributed to the protection of the perovskite film from decomposition.

Graphene QDs: Graphene QDs (GQDs) show exceptional optical and electrical properties because of their size-tuned optical response. In addition, GQDs show unusual properties when compared with conventional QDs such as biocompatibility, low toxicity, solubility, chemical stability, stable photoluminescence, etc.^[165,166] Gupta et al.^[167] first introduced luminescent

GQDs in OSCs by blending them with the conjugated polymers. Later, GQDs were incorporated as a third component in ternary OSCs, most notably QDs/silicon heterojunction solar cells, and in QD-sensitized solar cell applications.^[168] In PSCs, GQDs have been applied to TiO₂ and SnO₂ ETLs to improve the device performance by enhancing the electron extraction by effectively filling the electron traps as well as improving the conductivity of the active area/ETL interface.^[169,170] Moreover, the incorporation of GQDs into the perovskite layer helps in passivating the grain boundaries that also helped to facilitate electron extraction.^[171–173] Recently, Hosseini et al.^[174] studied optical modeling by coating luminescent GQDs as a DC layer on the front side of the photovoltaic device and found that the inclusion of GQDs enhanced the performance as well as suppressed UV light penetration into the cell. They also studied the effect on IPCE performance of different PLQE (6% and 94%) GQDs, along with their concentration and film thickness. Figure 10d shows the IPCE plots with and without 6% and 94% PLQE GQD luminescent layer. In the 300–400 nm wavelength range, the photon-to-current conversion percentage rises for 94% PLQE GQDs, and it is directly related to UV light to visible conversion. Bian et al.^[175] also introduced nitrogen-doped GQDs that showed PLQE up to 80% and helped to improve the photovoltaic and stability performance of PSCs. The PCE increased from 15.53% to 16.02% which is mainly due to an increase in *J*_{sc} from 18.67 to 19.15 mA cm⁻². The emission and absorption spectra of N-GQD

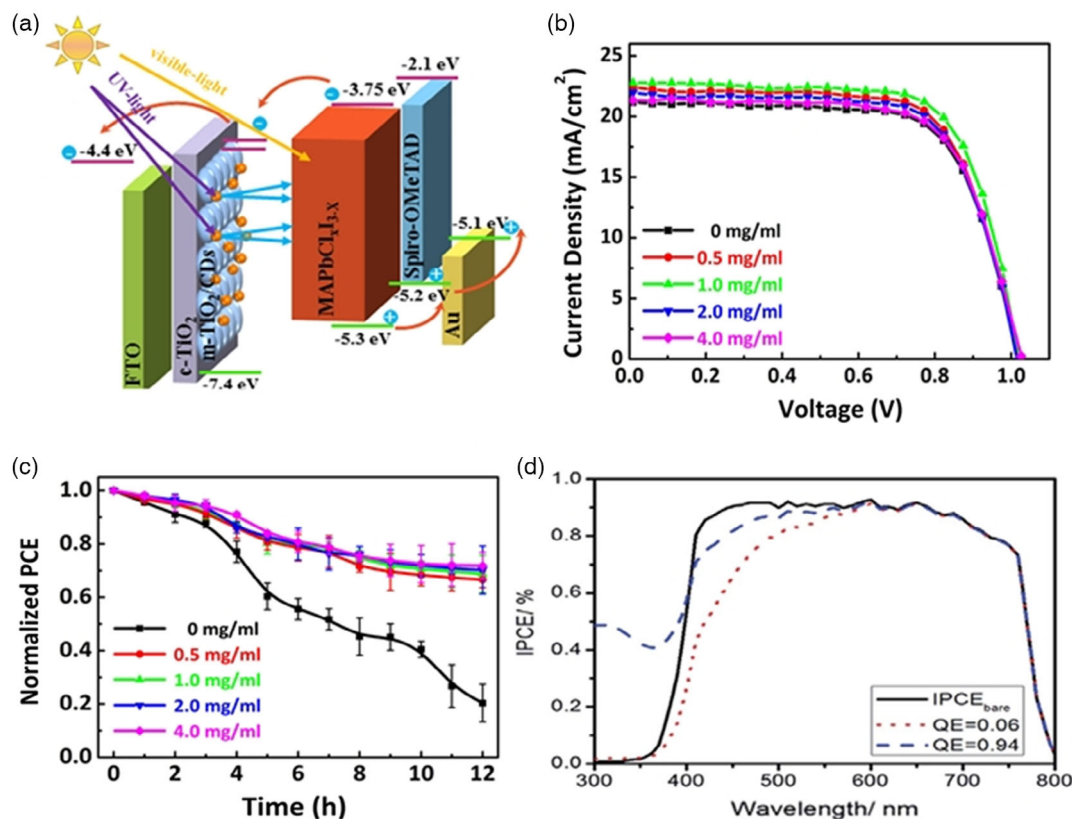


Figure 10. a) Device geometry with energy levels, b) *J*-*V* curve with and without fluorescent CD device, and c) reported stability of fluorescent CD-based devices under light irradiation for 12 h. Reproduced with permission.^[24] Copyright 2017, American Chemical Society. d) Reported IPCE with and without GQDs of 6% and 94% QEs. Reproduced under the terms of the CC-BY license (CC BY 3.0).^[174] Copyright 2018, the Authors. Published by Royal Society of Chemistry.

aqueous solution in the sp^2 domains' π - π^* transition peak occur at 255 nm, and the emission peak appears in the visible region (585 nm) wavelength, and under 385 nm UV light, the device is shown benefitting from the N-GQDs layer. Thus, the N-GQD cells show a significant improvement in J_{sc} when compared with the control devices. In addition, the N-GQD-based devices retain 98% PCE after 24 h of light irradiation, while the control only retains 95% of its initial value after.

3.2.4. Organic Molecules

The tunable optical and electrical properties of organic molecules by varying the highest occupied molecular orbital (HOMO) and lowest unoccupied molecular orbital (LUMO) energy levels make it attractive for organic photovoltaics, LEDs, transistors, photodetectors applications, etc.^[176–178] The properties can be altered by doing small changes to the molecular structure by varying the shape and size of molecules, and these molecules being solution processable and having low-cost deposition.^[179] There are several organic molecules that have been reported previously as ETL and HTL in PSCs.^[180–182] Recently, Bella et al.^[183] coated photopolymer on the front side of the device, as a UV-curable fluoropolymer layer. It provided an easy-cleaning benefit on the substrates' front side by forming a hydrophobic barrier to environmental moisture. This coating, also called V570, is defined as a

multifunction photopolymer layer that increases the photocurrent by 6% and increases the PCE up to 18.67% compared with 17.31% PCE of control devices. The optical properties of V570 are well matched with PSCs' device spectral response. It has an absorption peak in the UV region (377 nm) and photoemission in the visible region. The improvement in J_{sc} from 21.96 to 23.23 mA cm^{-2} clearly shows the benefit of V570 and how it helps with UV-to-visible light conversion. The stability measurement of the device of control and the coating of the luminescent polymer layer have been reported, for up to 6 months. In the first 3 months, the devices were tested in argon (Ar) atmosphere and for the next 3 months at outdoor conditions. In both conditions, the devices were kept under UV light irradiation. The efficiency of the DC layer-uncoated devices falls down rapidly within the first month, whereas the coated luminescent polymer layer device retained its PCE up to 80% of the initial performance for 3 months. Gheno et al.^[184] introduced the S-tetrazine (NITZ) molecule that contains polystyrene and N-(2-(6-chloro-tetrazin-3-yloxy)ethyl)-naphthalimide. The molecular structure of NITZ is shown in **Figure 11a**, where naphthalimide shows a good absorption coefficient and transferred energy to tetrazine via Forster mechanism. The NITZ showed favorable optical properties (**Figure 11b**) as a DC layer and has excitation in the UV while shown photoemission in the visible region. $\text{CH}_3\text{NH}_3\text{PbI}_{3-x}\text{Cl}_x$ perovskite layer was deposited

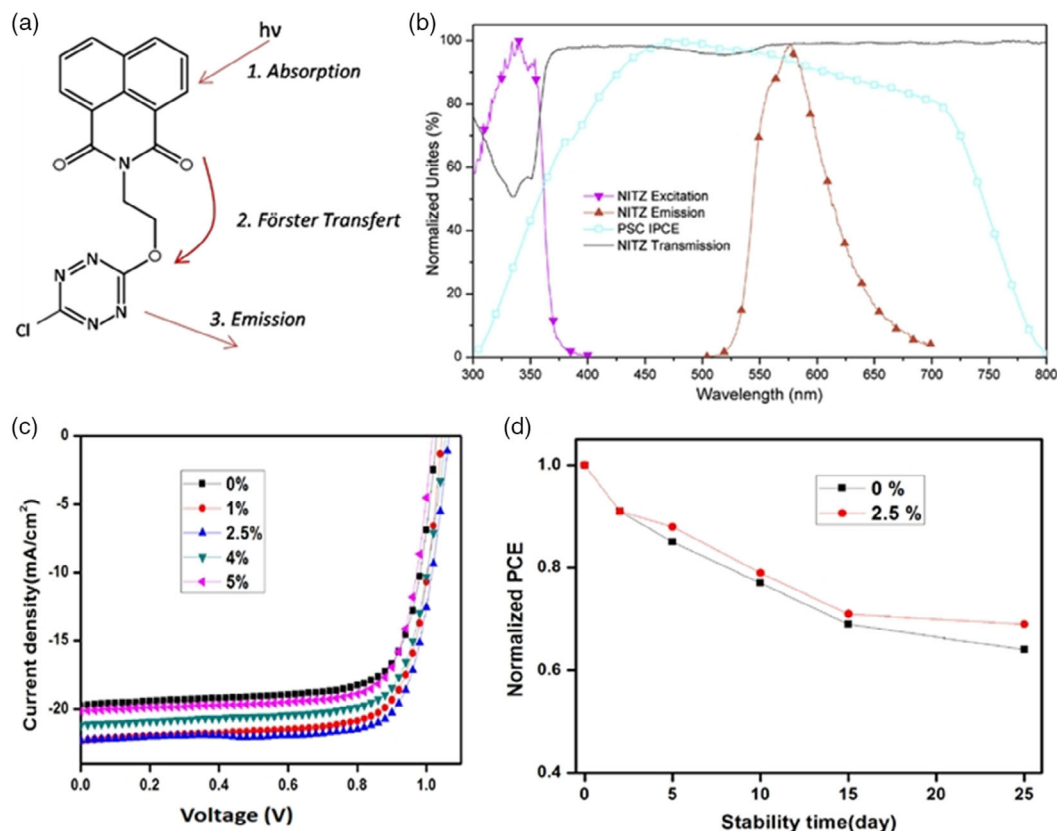


Figure 11. a) The structure of NITZ molecule with its photophysical mechanism and b) the NITZ molecule optical properties with PSC spectral response. Reproduced with permission,^[184] Copyright 2017, Elsevier B.V. c) J - V curve of reported devices at different concentrations of NPB in PTAA HTL layer and d) normalized PCE of control, and 2.5 wt% NPB devices for 25 days (under dark, RH40%). Reproduced with permission,^[185] Copyright 2020, International Solar Energy Society, Elsevier Ltd.

between a TiO₂/WO₃ and spiro-OMeTAD layer during device fabrications. The NITZ-coated film was placed between incident light and device during measuring the photovoltaic performance. It does not influence the PCE, whereas helped to improve device stability. Recently, Pathipati et al.^[185] merged a fluorescent *N,N'*-di (naphtha-1-yl)-*N,N'*-diphenyl-benzidine (NPB) organic molecule into HTL that also worked as a DC layer. Poly (triaryl amine) (PTAA) was used as polymeric HTL and the doping of NPB into it improved the charge carrier lifetime, reduced voltage losses, and enhanced cell stability. Moreover, the luminescent organic molecules between the HTL and perovskite layer help energy-level alignment for charge extractions as NPB has a deep HOMO level (−5.4 eV) that is close to perovskite HOMO level (−5.4 eV). This energy-level alignment also helped in improving the V_{oc} by reducing the voltage loss of 0.1 eV at the interface. Figure 11c shows the J - V characteristics which were reported at different concentrations of NPB and the optimized results were obtained at 2.5 wt% NPB in the PTAA HTL layer. The device with 2.5 wt% NPB obtained a PCE of 18.23%, and the J_{sc} , V_{oc} , and FF were measured as 22.32 mA cm^{−2}, 1.06 V, and 76.7%, respectively. These were the improved results than control device that had PCE, J_{sc} , V_{oc} , and FF of 15.18%, 19.76 mA cm^{−2}, 1.02 V, and 74.6%, respectively. The increase in J_{sc} , V_{oc} , and FF is due to the generation of additional charge carriers, energy band alignment, and improved film morphology. Moreover, the NPB-doped devices also showed a significant improvement in stability, as shown in Figure 11d. Therefore, in this case, slight doping of luminescent molecules into the HTL layer can add many benefits to PSCs.

4. Current Challenges and Future Perspectives

The PSCs have a big drawback in terms of limited efficiency as they aren't sensitive to the complete incident spectrum of sunlight. PSCs can utilize only a relatively small fraction of the solar incident photons with energy matching with the characteristic bandgap of the perovskite AL material. The demand to manage the improvement of UV light stability and simultaneous improvement in PSC performance are popular and still remain an important challenge. The use of DC materials is one of the approaches to improve the utilization of the incident spectrum. Due to it, the need for solution-processable, photostable, and cost-effective DC materials is increasing. Most of the lanthanide DC material synthesis processes required high temperature, and also their material availability on Earth are limited, which restrict them for future applications. The development of nonlanthanide DC materials can be an approach for future cost-effective device applications. From the device point of view, most DC materials have been applied to the front side of the transparent electrode as it may be difficult to maintain when depositing other films, and the additional deposition layer needs environmental protection and leads to an increase in overall costs. The focus should be needed to develop DC materials that can easily be doped in the charge transport or perovskite photoactive layer. Moreover, the future DC materials would need to have a dual-functional properties, that is, the DC materials may work as a DC layer and also facilitate charge carrier transport simultaneously. Besides this, future focus will also be on utilizing the whole incoming spectrum from IR to UV in photovoltaic devices.

The development of DC and UC mechanism by a single layer would be beneficial from a cost and performance improvement point of view. The implementation of UC and DC materials together could be an efficient process to improve the stability and efficiency of PSCs while also allowing for the reduction in overall device cost. Several DC and UC compounds with good energy transfer efficiency have been identified for solar applications.^[186–188] Similarly, materials with UV/IR absorption and visible emission may be researched and prepared to improve PSC efficiency. In terms of applicability, DC materials-based devices excel in fields where UV and near-blue visible light are not absorbed by photoactive layers. The UV radiation wavelengths emitted by Sun are classified as 100–280 nm (UV-C), 280–315 nm (UV-B), and 318–400 nm (UV-A). However, the energy reaching the Earth is in the range of 290–400 nm, in which the UV-C is entirely blocked by the ozone layer, and UV-B is ≈90%, absorbed by the Earth's atmosphere.^[189] There is an abundance of UV radiation accessible in space. The researchers are interested in exploring PSCs for space applications as space is devoid of oxygen and moisture, both of which are known to be harmful to the performance of perovskite photoactive layers.^[190–192] Apart from it, space has a greater concentration of high-intensity UV light than on the Earth's surface, and the insertion of DC materials into the devices will be very useful from the standpoint of improving PCE and stability.

5. Conclusion

The importance of photoconversion materials has been highlighted in terms of improving the photovoltaic performance of a variety of different PSCs and device architectures. In this review, we have summarized the importance of DC materials and their development for achieving spectral conversion in PSCs. In conclusion, we focused on DC materials made of lanthanides and nonlanthanides, their spectrum conversion features, working phenomena, and recent advances in PSCs for improving the stability and device performance. This review may allow researchers working on the PSCs to develop more photostable devices and consequently help in future commercialization in an increasingly green energy market. DC layers not only protect the devices from harmful UV light, but also modify the incident light to improve photocurrent generation. Furthermore, DC material doping in the CTL, or as a coating on top of it, could enhance the morphology of the CTL films and change the CTL energy-level band alignment. The morphology improvement helps to reduce the recombination at the CTL interfaces and that results in an enhancement of FF. The shifting of energy levels of CTL impacts the V_{oc} of the photovoltaic devices. By summarizing data from all reported work of lanthanide and nonlanthanide-based PSCs, it is clear that DC materials show huge impact on device performance and stability. PSCs with Eu³⁺ are frequently reported to exhibit an increase in efficiency and stability. Moreover, the Eu³⁺ DC-based devices not only show long-term UV light irradiation stability but also show stability in ambient environment and deliver multifunction benefits to PSCs. Recently researchers have focused toward replacing Eu³⁺ with Sm³⁺. Both show similar impact on improving device performance; however, the Eu³⁺ based devices are much more stable

under UV light irradiation and under ambient conditions. The reason behind the improved device performance with Eu^{3+} is the successful absorption of high-energy photons and their subsequent conversion to more favorable low-energy photons. PSCs also use yttrium, cerium, and terbium-based DC compounds, although their performance and stability enhancement are not as spectacular. Furthermore, their deposition techniques require a complicated high-temperature and high-vacuum environment, while Eu^{3+} - and Sm^{3+} -based compounds are solution processable. This is the primary prerequisite of a cost-effective manufacturing approach. In nonlanthanide DC materials, QDs are becoming increasingly popular for PSCs. It offers precise band tuning qualities as well as the ability to eliminate overlapping of the absorption and emission spectra. Likewise, ZnSe, CdSe, carbon QDs, and GQDs have been implemented to improve the PCE and stability of PSCs. Oxides and organic molecule nanophosphors have also contributed to increasing the J_{sc} and PCE by more than 7–18% of its initial value and provided additional stability to PSCs.

Acknowledgements

R.D. sincerely acknowledges the SPECIFIC Innovation and Knowledge Centre (EP/N020863/1) and ATIP (EP/T028513/1) grant for providing financial support. S.B. sincerely acknowledges the IIT Delhi for providing postdoctoral fellowship.

Conflict of Interest

The authors declare no conflict of interest.

Keywords

downconversion, lanthanides, nonlanthanides, perovskite solar cells, stabilities

Received: March 24, 2022

Revised: May 18, 2022

Published online:

- [1] N. S. Lewis, D. G. Nocera, *Proc. Natl. Acad. Sci.* **2006**, *103*, 15729.
- [2] S. Joshi, S. Mittal, P. Holloway, P. R. Shukla, B. Ó Gallachóir, J. Glynn, *Nat. Commun.* **2021**, *12*, 5738.
- [3] V. M. Fthenakis, H. C. Kim, E. Alsema, *Environ. Sci. Technol.* **2008**, *42*, 2168.
- [4] N. Liu, Q. Du, G. Yin, P. Liu, L. Li, H. Xie, C. Zhu, Y. Li, H. Zhou, W.-B. Zhang, Q. Chen, *J. Mater. Chem. A* **2018**, *6*, 6806.
- [5] D. Shi, V. Adinolfi, R. Comin, M. Yuan, E. Alarousu, A. Buin, Y. Chen, S. Hoogland, A. Rothenberger, K. Katsiev, Y. Losovyj, X. Zhang, P. A. Dowben, O. F. Mohammed, E. H. Sargent, O. M. Bakr, *Science*. **2015**, *347*, 519.
- [6] N.-G. Park, *Mater. Today* **2015**, *18*, 65.
- [7] P. Mahajan, R. Datt, W. Chung Tsoi, V. Gupta, A. Tomar, S. Arya, *Coord. Chem. Rev.* **2021**, *429*, 213633.
- [8] P. Mahajan, B. Padha, S. Verma, V. Gupta, R. Datt, W. C. Tsoi, S. Satapathi, S. Arya, *J. Energy Chem.* **2022**, *68*, 330.
- [9] A. Kojima, K. Teshima, Y. Shirai, T. Miyasaka, *J. Am. Chem. Soc.* **2009**, *131*, 6050.
- [10] H. Min, D. Y. Lee, J. Kim, G. Kim, K. S. Lee, J. Kim, M. J. Paik, Y. K. Kim, K. S. Kim, M. G. Kim, T. J. Shin, S. Il Seok, *Nature* **2021**, *598*, 444.
- [11] J. Jeong, M. Kim, J. Seo, H. Lu, P. Ahlawat, A. Mishra, Y. Yang, M. A. Hope, F. T. Eickemeyer, M. Kim, Y. J. Yoon, I. W. Choi, B. P. Darwich, S. J. Choi, Y. Jo, J. H. Lee, B. Walker, S. M. Zakeeruddin, L. Emsley, U. Rothlisberger, A. Hagfeldt, D. S. Kim, M. Grätzel, J. Y. Kim, *Nature* **2021**, *592*, 381.
- [12] H. F. Zarick, N. Soetan, W. R. Erwin, R. Bardhan, *J. Mater. Chem. A* **2018**, *6*, 5507.
- [13] J. H. Noh, S. H. Im, J. H. Heo, T. N. Mandal, S. Il Seok, *Nano Lett.* **2013**, *13*, 1764.
- [14] C. J. Bartel, C. Sutton, B. R. Goldsmith, R. Ouyang, C. B. Musgrave, L. M. Ghiringhelli, M. Scheffler, *Sci. Adv.* **2019**, *5*, eaav0693.
- [15] Y. Fan, H. Qin, W. Ye, M. Liu, F. Huang, D. Zhong, *Thin Solid Films* **2018**, *667*, 40.
- [16] I. Mesquita, L. Andrade, A. Mendes, *Renew. Sustain. Energy Rev.* **2018**, *82*, 2471.
- [17] J. Meiss, K. Leo, M. K. Riede, C. Uhrich, W.-M. Gnehr, S. Sonntag, M. Pfeiffer, *Appl. Phys. Lett.* **2009**, *95*, 213306.
- [18] M. Li, H. Li, J. Fu, T. Liang, W. Ma, *J. Phys. Chem. C* **2020**, *124*, 27251.
- [19] D. Wang, M. Wright, N. K. Elumalai, A. Uddin, *Sol. Energy Mater. Sol. Cells* **2016**, *147*, 255.
- [20] D. Bryant, N. Aristidou, S. Pont, I. Sanchez-Molina, T. Chotchunangatchaval, S. Wheeler, J. R. Durrant, S. A. Haque, *Energy Environ. Sci.* **2016**, *9*, 1655.
- [21] N. U. Rahman, W. U. Khan, S. Khan, X. Chen, J. Khan, J. Zhao, Z. Yang, M. Wu, Z. Chi, *J. Mater. Chem. A* **2019**, *7*, 6467.
- [22] A. A. Zaky, E. Christopoulos, K. Gkini, M. K. Arfanis, L. Sygellou, A. Kaltzoglou, A. Stergiou, N. Tagmatarchis, N. Balis, P. Falaras, *Appl. Catal. B Environ.* **2021**, *284*, 119714.
- [23] G. Niu, X. Guo, L. Wang, *J. Mater. Chem. A* **2015**, *3*, 8970.
- [24] J. Jin, C. Chen, H. Li, Y. Cheng, L. Xu, B. Dong, H. Song, Q. Dai, *ACS Appl. Mater. Interfaces* **2017**, *9*, 14518.
- [25] T. Leijtens, G. E. Eperon, S. Pathak, A. Abate, M. M. Lee, H. J. Snaith, *Nat. Commun.* **2013**, *4*, 2885.
- [26] W. Li, W. Zhang, S. Van Reenen, R. J. Sutton, J. Fan, A. A. Haghighirad, M. B. Johnston, L. Wang, H. J. Snaith, *Energy Environ. Sci.* **2016**, *9*, 490.
- [27] J. Ji, X. Liu, H. Jiang, M. Duan, B. Liu, H. Huang, D. Wei, Y. Li, M. Li, *iScience* **2020**, *23*, 101013.
- [28] S. S. Shin, W. S. Yang, J. H. Noh, J. H. Suk, N. J. Jeon, J. H. Park, J. S. Kim, W. M. Seong, S. Il Seok, *Nat. Commun.* **2015**, *6*, 7410.
- [29] L. Zhu, Z. Shao, J. Ye, X. Zhang, X. Pan, S. Dai, *Chem. Commun.* **2016**, *52*, 970.
- [30] C. D. Wessendorf, J. Hanisch, D. Müller, E. Ahlswede, *Sol. RRL* **2018**, *2*, 1800056.
- [31] J. Dong, J. Wu, J. Jia, X. He, Z. Lan, L. Fan, J. Lin, M. Huang, *ChemSusChem* **2018**, *11*, 619.
- [32] J. Zhou, R. Zhou, J. Zhu, P. Jiang, L. Wan, H. Niu, L. Hu, X. Yang, J. Xu, B. Xu, *Sol. RRL* **2021**, *5*, 2100494.
- [33] M. Neophytou, M. De Bastiani, N. Gasparini, E. Aydin, E. Ugur, A. Seitkhan, F. Moruzzi, Y. Choiaie, A. J. Ramadan, J. R. Troughton, R. Hallani, A. Savva, L. Tsetseris, S. Inal, D. Baran, F. Laquai, T. D. Anthopoulos, H. J. Snaith, S. De Wolf, I. McCulloch, *ACS Appl. Energy Mater.* **2019**, *2*, 8090.
- [34] D. Zheng, G. Wang, W. Huang, B. Wang, W. Ke, J. L. Logsdon, H. Wang, Z. Wang, W. Zhu, J. Yu, M. R. Wasielewski, M. G. Kanatzidis, T. J. Marks, A. Facchetti, *Adv. Funct. Mater.* **2019**, *29*, 1900265.
- [35] F. Paquin, J. Rivnay, A. Salleo, N. Stingelin, C. Silva-Acuña, *J. Mater. Chem. C* **2015**, *3*, 10715.

- [36] X. Luo, T. Wu, Y. Wang, X. Lin, H. Su, Q. Han, L. Han, *Sci. China Chem.* **2021**, *64*, 218.
- [37] Wei Qin, Yuliang Zhang, Wei Zi, Zhou Yang, Dong Yang, Pengcheng Ding, Wei Yu, Shengzhong Liu, Can Li, In *2015 IEEE 42nd Photovoltaic Specialist Conference (PVSC)*, IEEE, Piscataway, NJ **2015**; pp. 1–5.
- [38] Z. Zhang, Z. Li, L. Meng, S. Lien, P. Gao, *Adv. Funct. Mater.* **2020**, *30*, 2001904.
- [39] M. Jošt, L. Kegelmann, L. Korte, S. Albrecht, *Adv. Energy Mater.* **2020**, *10*, 1904102.
- [40] Z. Fang, Q. Zeng, C. Zuo, L. Zhang, H. Xiao, M. Cheng, F. Hao, Q. Bao, L. Zhang, Y. Yuan, W.-Q. Wu, D. Zhao, Y. Cheng, H. Tan, Z. Xiao, S. Yang, F. Liu, Z. Jin, J. Yan, L. Ding, *Sci. Bull.* **2021**, *66*, 621.
- [41] Q. Lin, A. Armin, R. C. R. Nagiri, P. L. Burn, P. Meredith, *Nat. Photonics* **2015**, *9*, 106.
- [42] S.-W. Lee, S. Kim, S. Bae, K. Cho, T. Chung, L. E. Mundt, S. Lee, S. Park, H. Park, M. C. Schubert, S. W. Glunz, Y. Ko, Y. Jun, Y. Kang, H.-S. Lee, D. Kim, *Sci. Rep.* **2016**, *6*, 38150.
- [43] J.-W. Lee, D.-J. Seol, A.-N. Cho, N.-G. Park, *Adv. Mater.* **2014**, *26*, 4991.
- [44] S. Agarwal, P. R. Nair, *J. Appl. Phys.* **2018**, *124*, 183101.
- [45] M. J. Taghavi, M. Houshmand, M. H. Zandi, N. E. Gorji, *Superlattices Microstruct.* **2016**, *97*, 424.
- [46] D.-L. Wang, H.-J. Cui, G.-J. Hou, Z.-G. Zhu, Q.-B. Yan, G. Su, *Sci. Rep.* **2016**, *6*, 18922.
- [47] K. Wojciechowski, T. Leijtens, S. Siprova, C. Schlueter, M. T. Hörantner, J. T.-W. Wang, C.-Z. Li, A. K.-Y. Jen, T.-L. Lee, H. J. Snaith, *J. Phys. Chem. Lett.* **2015**, *6*, 2399.
- [48] L. Duan, A. Uddin, *Mater. Chem. Front.* **2022**, *6*, 400.
- [49] X.-X. Gao, B. Ding, H. Kanda, Z. Fei, W. Luo, Y. Zhang, N. Shibayama, A. Züttel, F. F. Tirani, R. Scopelliti, S. Kinge, B. Zhang, Y. Feng, P. J. Dyson, M. K. Nazeeruddin, *Cell Reports Phys. Sci.* **2021**, *2*, 100475.
- [50] T. Yang, N. J. Jeon, H. Shin, S. S. Shin, Y. Y. Kim, J. Seo, *Adv. Sci.* **2019**, *6*, 1900528.
- [51] S. Mazumdar, Y. Zhao, X. Zhang, *Front. Electron.* **2021**, *2*, 1.
- [52] S. Shao, M. A. Loi, *Adv. Mater. Interfaces* **2020**, *7*, 1901469.
- [53] J. You, L. Meng, T.-B. Song, T.-F. Guo, Y. (Michael) Yang, W.-H. Chang, Z. Hong, H. Chen, H. Zhou, Q. Chen, Y. Liu, N. De Marco, Y. Yang, *Nat. Nanotechnol.* **2016**, *11*, 75.
- [54] W. Chen, Y. Wu, Y. Yue, J. Liu, W. Zhang, X. Yang, H. Chen, E. Bi, I. Ashraf, M. Grätzel, L. Han, *Science* **2015**, *350*, 944.
- [55] N. Ahn, K. Kwak, M. S. Jang, H. Yoon, B. Y. Lee, J.-K. Lee, P. V. Pikhitsa, J. Byun, M. Choi, *Nat. Commun.* **2016**, *7*, 13422.
- [56] J.-W. Lee, D.-H. Kim, H.-S. Kim, S.-W. Seo, S. M. Cho, N.-G. Park, *Adv. Energy Mater.* **2015**, *5*, 1501310.
- [57] Q. Sun, P. Fassel, D. Becker-Koch, A. Bausch, B. Rivkin, S. Bai, P. E. Hopkinson, H. J. Snaith, Y. Vaynzof, *Adv. Energy Mater.* **2017**, *7*, 1700977.
- [58] S. Zhang, G. Han, *Prog. Energy* **2020**, *2*, 022002.
- [59] C. Chen, H. Li, J. Jin, X. Chen, Y. Cheng, Y. Zheng, D. Liu, L. Xu, H. Song, Q. Dai, *Adv. Energy Mater.* **2017**, *7*, 1700758.
- [60] S. K. Karunakaran, G. M. Arumugam, W. Yang, S. Ge, S. N. Khan, X. Lin, G. Yang, *ACS Sustain. Chem. Eng.* **2021**, *9*, 1035.
- [61] L. Chen, W. Wu, J. Wang, Z. Qian, R. Liu, Y. Niu, Y. Chen, X. Xie, H. Zhang, *ACS Appl. Energy Mater.* **2021**, *4*, 3937.
- [62] R. Sun, D. Zhou, H. Song, *Nano Sel.* **2022**, *3*, 531.
- [63] Z. Song, W. Xu, Y. Wu, S. Liu, W. Bi, X. Chen, H. Song, *Small* **2020**, *16*, 2001770.
- [64] J. Duan, Y. Zhao, X. Yang, Y. Wang, B. He, Q. Tang, *Adv. Energy Mater.* **2018**, *8*, 1.
- [65] G. Pan, X. Bai, D. Yang, X. Chen, P. Jing, S. Qu, L. Zhang, D. Zhou, J. Zhu, W. Xu, B. Dong, H. Song, *Nano Lett.* **2017**, *17*, 8005.
- [66] Q. Hu, Z. Li, Z. Tan, H. Song, C. Ge, G. Niu, J. Han, J. Tang, *Adv. Opt. Mater.* **2018**, *6*, 1700864.
- [67] S. Liu, J. Lyu, D. Zhou, X. Zhuang, Z. Shi, R. Sun, L. Liu, Y. Wu, B. Liu, D. Liu, H. Song, *Adv. Funct. Mater.* **2022**, *32*, 2112647.
- [68] J. Shi, F. Li, J. Yuan, X. Ling, S. Zhou, Y. Qian, W. Ma, *J. Mater. Chem. A* **2019**, *7*, 20936.
- [69] S. Kachhap, S. Singh, A. K. Singh, S. K. Singh, *J. Mater. Chem. C* **2022**, *10*, 3647.
- [70] W. J. Mir, T. Sheikh, H. Arfin, Z. Xia, A. Nag, *NPG Asia Mater.* **2020**, *12*, 9.
- [71] T. Liang, J. Fu, M. Li, H. Li, Y. Hao, W. Ma, *Mater. Today Energy* **2021**, *21*, 100740.
- [72] D. Ma, Y. Shen, T. Su, J. Zhao, N. U. Rahman, Z. Xie, F. Shi, S. Zheng, Y. Zhang, Z. Chi, *Mater. Chem. Front.* **2019**, *3*, 2058.
- [73] L. Ruan, Y. Zhang, *Nat. Commun.* **2021**, *12*, 219.
- [74] W. Shockley, H. J. Queisser, *J. Appl. Phys.* **1961**, *32*, 510.
- [75] T. Trupke, M. A. Green, P. Würfel, *J. Appl. Phys.* **2002**, *92*, 1668.
- [76] A. Luque, A. Martí, *Phys. Rev. Lett.* **1997**, *78*, 5014.
- [77] R. Brendel, J. Werner, H. Queisser, *Sol. Energy Mater. Sol. Cells* **1996**, *41–42*, 419.
- [78] J. de Wild, A. Meijerink, J. K. Rath, W. G. J. H. M. van Sark, R. E. I. Schropp, *Energy Environ. Sci.* **2011**, *4*, 4835.
- [79] T. Forster, *Naturwissenschaften* **1946**, *33*, 166.
- [80] D. L. Dexter, *J. Chem. Phys.* **1953**, *21*, 836.
- [81] P. P. Boix, K. Nonomura, N. Mathews, S. G. Mhaisalkar, *Mater. Today* **2014**, *17*, 16.
- [82] S. P. Dunfield, L. Bliss, F. Zhang, J. M. Luther, K. Zhu, M. F. A. M. Hest, M. O. Reese, J. J. Berry, *Adv. Energy Mater.* **2020**, *10*, 1904054.
- [83] Q. Wali, N. K. Elumalai, Y. Iqbal, A. Uddin, R. Jose, *Renew. Sustain. Energy Rev.* **2018**, *84*, 89.
- [84] J. Y. Kim, J.-W. Lee, H. S. Jung, H. Shin, N.-G. Park, *Chem. Rev.* **2020**, *120*, 7867.
- [85] P. Lin, A. Loganathan, I. Raifuku, M. Li, Y. Chiu, S. Chang, A. Fakharuddin, C. Lin, T. Guo, L. Schmidt-Mende, P. Chen, *Adv. Energy Mater.* **2021**, *11*, 2100818.
- [86] A. Fakharuddin, L. Schmidt-Mende, G. Garcia-Belmonte, R. Jose, I. Mora-Sero, *Adv. Energy Mater.* **2017**, *7*, 1700623.
- [87] Y.-H. Zhang, Y. Li, *Rare Met.* **2021**, *40*, 2993.
- [88] M. L. Cable, D. J. Levine, J. P. Kirby, H. B. Gray, A. Ponce, *Adv. Inorg. Chem.* **2011**, *63*, 1.
- [89] A. de Bettencourt-Dias, *Dalton Trans.* **2007**, 2229.
- [90] Y. Hasegawa, Y. Kitagawa, T. Nakanishi, *NPG Asia Mater.* **2018**, *10*, 52.
- [91] David R. Wilburn, *USGS* **2012**, 15.
- [92] X. Huang, G. Zhang, A. Pan, F. Chen, C. Zheng, *Earth's Future* **2016**, *4*, 532.
- [93] H. Zhu, C. C. Lin, W. Luo, S. Shu, Z. Liu, Y. Liu, J. Kong, E. Ma, Y. Cao, R.-S. Liu, X. Chen, *Nat. Commun.* **2014**, *5*, 4312.
- [94] E. Polikarpov, D. Catalini, A. Padmaperuma, P. Das, T. Lemmon, B. Arey, C. A. Fernandez, *Opt. Mater.* **2015**, *46*, 614.
- [95] B. S. Richards, *Sol. Energy Mater. Sol. Cells* **2006**, *90*, 2329.
- [96] R. Datt, S. Bishnoi, H. K. H. Lee, S. Arya, S. Gupta, V. Gupta, W. C. Tsoi, *Aggregate* **2022**, *1*.
- [97] Q. G. Du, G. Shen, S. John, *AIP Adv.* **2016**, *6*, 065002.
- [98] M. A. Mohebbpour, M. Saffari, H. R. Soleimani, M. B. Tagani, *Phys. E Low-Dimens. Syst. Nanostruct.* **2018**, *97*, 282.
- [99] N. Chander, A. F. Khan, P. S. Chandrasekhar, E. Thouti, S. K. Swami, V. Dutta, V. K. Komarala, *Appl. Phys. Lett.* **2014**, *105*, 033904.
- [100] C. K. Huang, Y. C. Chen, W. B. Hung, T. M. Chen, K. W. Sun, W.-L. Chang, *Prog. Photovolt. Res. Appl.* **2013**, *21*, 1507.
- [101] W. Xu, H. Song, D. Yan, H. Zhu, Y. Wang, S. Xu, X. Bai, B. Dong, Y. Liu, *J. Mater. Chem.* **2011**, *21*, 12331.

- [102] J. Jin, H. Li, C. Chen, B. Zhang, W. Bi, Z. Song, L. Xu, B. Dong, H. Song, Q. Dai, *ACS Appl. Energy Mater.* **2018**, *1*, 2096.
- [103] R. Zhang, H. Lin, Y. Yu, D. Chen, J. Xu, Y. Wang, *Laser Photon. Rev.* **2014**, *8*, 158.
- [104] H.-S. Roh, G. S. Han, S. Lee, S. Kim, S. Choi, C. Yoon, J.-K. Lee, *J. Power Sources* **2018**, *389*, 135.
- [105] W. Bi, Y. Wu, B. Zhang, J. Jin, H. Li, L. Liu, L. Xu, Q. Dai, C. Chen, H. Song, *ACS Appl. Mater. Interfaces* **2019**, *11*, 11481.
- [106] H. Li, C. Chen, J. Jin, W. Bi, B. Zhang, X. Chen, L. Xu, D. Liu, Q. Dai, H. Song, *Nano Energy* **2018**, *50*, 699.
- [107] A. Zhang, N. Sun, L. Li, Y. Yang, X. Zhao, H. Jia, X. Liu, B. Xu, *J. Mater. Chem. C* **2015**, *3*, 9933.
- [108] W. Chen, Q. Luo, C. Zhang, J. Shi, X. Deng, L. Yue, Z. Wang, X. Chen, S. Huang, *J. Mater. Sci. Mater. Electron.* **2017**, *28*, 11346.
- [109] X. Liu, S. Chen, X. Wang, *J. Lumin.* **2007**, *127*, 650.
- [110] K. Mahmood, B. S. Swain, A. Amassian, *Adv. Energy Mater.* **2015**, *5*, 1500568.
- [111] N. U. Rahman, W. U. Khan, W. Li, S. Khan, J. Khan, S. Zheng, T. Su, J. Zhao, M. P. Aldred, Z. Chi, *J. Mater. Chem. A* **2019**, *7*, 322.
- [112] P. M. Aneesh, K. M. Krishna, M. K. Jayaraj, *J. Electrochem. Soc.* **2009**, *156*, K33.
- [113] K. Somasundaram, K. G. Girija, P. C. Selvin, V. Sudarsan, R. M. Kadam, R. K. Vatsa, *J. Lumin.* **2017**, *185*, 145.
- [114] I.-K. Jeong, H. L. Park, S. Mho, *Solid State Commun.* **1998**, *105*, 179.
- [115] X. Hou, T. Xuan, H. Sun, X. Chen, H. Li, L. Pan, *Sol. Energy Mater. Sol. Cells* **2016**, *149*, 121.
- [116] Z. Wang, F. Tao, W. Cai, L. Yao, X.-G. Li, *Bull. Mater. Sci.* **2011**, *34*, 1371.
- [117] P. Du, X. Huang, J. S. Yu, *Dye. Pigment.* **2018**, *153*, 307.
- [118] M. Ran, N. Liu, H. Yang, R. Meng, M. Chen, H. Lu, Y. Yang, *Appl. Phys. Lett.* **2020**, *116*, 113503.
- [119] L. Jiang, W. Chen, J. Zheng, L. Zhu, L. Mo, Z. Li, L. Hu, T. Hayat, A. Alsaedi, C. Zhang, S. Dai, *ACS Appl. Mater. Interfaces* **2017**, *9*, 26958.
- [120] J. Jia, J. Dong, J. Lin, Z. Lan, L. Fan, J. Wu, *J. Mater. Chem. C* **2019**, *7*, 937.
- [121] R. Ianoş, R. Băbuşă, R. Lazău, *Ceram. Int.* **2014**, *40*, 12207.
- [122] V. H. Mudavakkat, V. V. Atuchin, V. N. Kruchinin, A. Kayani, C. V. Ramana, *Opt. Mater.* **2012**, *34*, 893.
- [123] C. A. Traina, J. Schwartz, *Langmuir* **2007**, *23*, 9158.
- [124] G. Bohus, V. Hornok, A. Oszkó, A. Vértes, E. Kuzmann, I. Dékány, *Colloids Surf. A Physicochem. Eng. ASP.* **2012**, *405*, 6.
- [125] J. L. Ferrari, M. A. Cebim, A. M. Pires, M. A. Couto dos Santos, M. R. Davolos, *J. Solid State Chem.* **2010**, *183*, 2110.
- [126] C. W. Kim, T. Y. Eom, I. S. Yang, B. S. Kim, W. I. Lee, Y. S. Kang, Y. S. Kang, *Sci. Rep.* **2017**, *7*, 6849.
- [127] A. P. Jadhav, A. U. Pawar, U. Pal, Y. S. Kang, *J. Mater. Chem. C* **2014**, *496*.
- [128] M. Ammam, *J. Mater. Chem. A* **2013**, *1*, 6291.
- [129] N. I. Gumerova, A. Rompel, *Nat. Rev. Chem.* **2018**, *2*, 0112.
- [130] R. Tao, W. Fang, F. Li, Z. Sun, L. Xu, *J. Alloys Compd.* **2020**, *823*, 153738.
- [131] P. Song, P. Zhu, C. Zhang, *J. Alloys Compd.* **2018**, *731*, 1009.
- [132] L. Xiong, Y. Guo, J. Wen, H. Liu, G. Yang, P. Qin, G. Fang, *Adv. Funct. Mater.* **2018**, *28*, 1802757.
- [133] D. Yang, R. Yang, K. Wang, C. Wu, X. Zhu, J. Feng, X. Ren, G. Fang, S. Priya, S. Liu, *Nat. Commun.* **2018**, *9*, 3239.
- [134] L. P. Singh, M. N. Luwang, S. K. Srivastava, *New J. Chem.* **2014**, *38*, 115.
- [135] D. Yadav, U. Kumar, S. Upadhyay, *J. Adv. Ceram.* **2019**, *8*, 377.
- [136] J. Gomes, A. M. Pires, O. A. Serra, *Quim. Nova* **2004**, *27*, 706.
- [137] T. Grzyb, A. Szczeszak, J. Rozowska, J. Legendziewicz, S. Lis, *J. Phys. Chem. C* **2012**, *116*, 3219.
- [138] C. Zhang, J. Shi, X. Yang, L. Lu, X. Wang, *J. Rare Earths* **2010**, *28*, 513.
- [139] K. Suresh, K. V. R. Murthy, C. A. Rao, N. V. P. Rao, B. S. Rao, *J. Lumin.* **2013**, *133*, 96.
- [140] A. J. Haider, Z. N. Jameel, I. H. M. Al-Hussaini, *Energy Proc.* **2019**, *157*, 17.
- [141] T.-H. Zhang, L.-Y. Piao, S.-L. Zhao, Z. Xu, Q. Wu, C. Kong, *Chinese Phys. B* **2012**, *21*, 118401.
- [142] Q. G. Zeng, Z. J. Ding, Z. M. Zhang, *J. Lumin.* **2006**, *118*, 301.
- [143] W. Luo, R. Li, X. Chen, *J. Phys. Chem. C* **2009**, *113*, 8772.
- [144] L. Jiang, J. Zheng, W. Chen, Y. Huang, L. Hu, T. Hayat, A. Alsaedi, C. Zhang, S. Dai, *ACS Appl. Energy Mater.* **2018**, *1*, 93.
- [145] D. Falcomer, M. Daldosso, C. Cannas, A. Musinu, B. Lasio, S. Enzo, A. Speghini, M. Bettinelli, *J. Solid State Chem.* **2006**, *179*, 2452.
- [146] B. Zhang, Z. Song, J. Jin, W. Bi, H. Li, C. Chen, Q. Dai, L. Xu, H. Song, *J. Colloid Interface Sci.* **2019**, *553*, 14.
- [147] P. Chen, Z. Wang, S. Wang, M. Lyu, M. Hao, M. Ghasemi, M. Xiao, J.-H. Yun, Y. Bai, L. Wang, *Nano Energy* **2020**, *69*, 104392.
- [148] S. Gai, C. Li, P. Yang, J. Lin, *Chem. Rev.* **2014**, *114*, 2343.
- [149] J. H. Ma, C. W. Bark, H. W. Choi, *J. Nanosci. Nanotechnol.* **2018**, *19*, 1615.
- [150] J. Cui, P. Li, Z. Chen, K. Cao, D. Li, J. Han, Y. Shen, M. Peng, Y. Q. Fu, M. Wang, *Appl. Phys. Lett.* **2016**, *109*, 171103.
- [151] K. E. Jasim, in *Solar Cells – New Approaches and Reviews*, Vol. *i*, InTech, London, UK **2015**, p. 13.
- [152] E. H. M. Sakho, O. S. Oluwafemi, in *Nanomaterials for Solar Cell Applications*, Elsevier Inc. Amsterdam **2019**, pp. 377–415.
- [153] Q. Wang, X. Zhang, Z. Jin, J. Zhang, Z. Gao, Y. Li, S. F. Liu, *ACS Energy Lett.* **2017**, *2*, 1479.
- [154] S. H. Lee, C. Jung, Y. Jun, S.-W. Kim, *Opt. Mater.* **2015**, *49*, 230.
- [155] J.-Y. Jung, K. Zhou, J. H. Bang, J.-H. Lee, *J. Phys. Chem. C* **2012**, *116*, 12409.
- [156] B. Wang, B. Li, T. Shen, M. Li, J. Tian, *J. Energy Chem.* **2018**, *27*, 736.
- [157] M. M. Rahman, M. R. Karim, H. F. Alharbi, B. Aldokhayel, T. Uzzaman, H. Zahir, *Chem.* **2021**, *16*, 902.
- [158] J. M. AlGhamdi, S. AlOmar, M. A. Gondal, R. Moqbel, M. A. Dastageer, *Sol. Energy* **2020**, *209*, 108.
- [159] M. M. Tavakoli, H. T. Dastjerdi, D. Prochowicz, P. Yadav, R. Tavakoli, M. Saliba, Z. Fan, *J. Mater. Chem. A* **2019**, *7*, 14753.
- [160] M. M. Tavakoli, D. Prochowicz, P. Yadav, R. Tavakoli, *Phys. Status Solidi RRL* **2020**, *14*, 2000062.
- [161] C. Lee, X. Wei, J. W. Kysar, J. Hone, *Science* **2008**, *321*, 385.
- [162] Nguyen Nguyen, Le Nguyen, Ly Vo, Le Kim, *Polymers* **2019**, *11*, 1858.
- [163] J. B. Essner, G. A. Baker, *Environ. Sci. Nano* **2017**, *4*, 1216.
- [164] Z. Ku, Y. Rong, M. Xu, T. Liu, H. Han, *Sci. Rep.* **2013**, *3*, 3132.
- [165] L. Li, G. Wu, G. Yang, J. Peng, J. Zhao, J.-J. Zhu, *Nanoscale* **2013**, *5*, 4015.
- [166] S.-H. Choi, *J. Phys. D: Appl. Phys.* **2017**, *50*, 103002.
- [167] V. Gupta, N. Chaudhary, R. Srivastava, G. D. Sharma, R. Bhardwaj, S. Chand, *J. Am. Chem. Soc.* **2011**, *133*, 9960.
- [168] S. J. Sung, J. H. Kim, S. H. Gihm, J. Park, Y. S. Cho, S. J. Yang, C. R. Park, *ACS Appl. Energy Mater.* **2019**, *2*, 8826.
- [169] J. Xie, K. Huang, X. Yu, Z. Yang, K. Xiao, Y. Qiang, X. Zhu, L. Xu, P. Wang, C. Cui, D. Yang, *ACS Nano* **2017**, *11*, 9176.
- [170] J. Ryu, J. W. Lee, H. Yu, J. Yun, K. Lee, J. Lee, D. Hwang, J. Kang, S. K. Kim, J. Jang, *J. Mater. Chem. A* **2017**, *5*, 16834.
- [171] S. Pang, C. Zhang, H. Zhang, H. Dong, D. Chen, W. Zhu, H. Xi, J. Chang, Z. Lin, J. Zhang, Y. Hao, *Appl. Surf. Sci.* **2020**, *507*, 145099.
- [172] Z. Zhu, J. Ma, Z. Wang, C. Mu, Z. Fan, L. Du, Y. Bai, L. Fan, H. Yan, D. L. Phillips, S. Yang, *J. Am. Chem. Soc.* **2014**, *136*, 3760.
- [173] X. Fang, J. Ding, N. Yuan, P. Sun, M. Lv, G. Ding, C. Zhu, *Phys. Chem. Chem. Phys.* **2017**, *19*, 6057.
- [174] Z. Hosseini, T. Ghanbari, *RSC Adv.* **2018**, *8*, 31502.

- [175] H. Bian, Q. Wang, S. Yang, C. Yan, H. Wang, L. Liang, Z. Jin, G. Wang, S. (Frank) Liu, *J. Mater. Chem. A* **2019**, *7*, 5740.
- [176] D. Yang, D. Ma, *Adv. Opt. Mater.* **2019**, *7*, 1800522.
- [177] S.-J. Zou, Y. Shen, F.-M. Xie, J.-D. Chen, Y.-Q. Li, J.-X. Tang, *Mater. Chem. Front.* **2020**, *4*, 788.
- [178] U. Zschieschang, H. Klauk, *J. Mater. Chem. C* **2019**, *7*, 5522.
- [179] A. Soultati, A. Verykios, K.-K. Armadorou, M. Tountas, V. P. Vidali, K. Ladomenou, L. Palilis, D. Davazoglou, A. G. Coutsolelos, P. Argitis, M. Vasilopoulou, *J. Phys. D. Appl. Phys.* **2020**, *53*, 263001.
- [180] R. Xue, M. Zhang, D. Luo, W. Chen, R. Zhu, Y. (Michael) Yang, Y. Li, Y. Li, *Sci. China Chem.* **2020**, *63*, 987.
- [181] S. A. Ok, B. Jo, S. Somasundaram, H. J. Woo, D. W. Lee, Z. Li, B.-G. Kim, J. H. Kim, Y. J. Song, T. K. Ahn, S. Park, H. J. Park, *Nat. Commun.* **2018**, *9*, 4537.
- [182] H. Wang, F. Yang, N. Li, J. Song, J. Qu, S. Hayase, W.-Y. Wong, *Chem. Eng. J.* **2020**, *392*, 123677.
- [183] F. Bella, G. Griffini, J.-P. Correa-Baena, G. Saracco, M. Grätzel, A. Hagfeldt, S. Turri, C. Gerbaldi, *Science* **2016**, *354*, 203.
- [184] A. Gheno, T. Trigaud, J. Bouclé, P. Audebert, B. Ratier, S. Vedraïne, *Opt. Mater.* **2018**, *75*, 781.
- [185] S. R. Pathipati, M. N. Shah, X. Pan, *Sol. Energy* **2020**, *197*, 363.
- [186] P. A. Loiko, N. M. Khaidukov, J. Méndez-Ramos, E. V. Vilejshikova, N. A. Skoptsov, K. V. Yumashev, *J. Lumin.* **2016**, *170*, 1.
- [187] A. Bahadur, R. S. Yadav, R. V. Yadav, S. B. Rai, *J. Solid State Chem.* **2017**, *246*, 81.
- [188] K.-T. Lee, J.-H. Park, S. J. Kwon, H.-K. Kwon, J. Kyhm, K.-W. Kwak, H. S. Jang, S. Y. Kim, J. S. Han, S.-H. Lee, D.-H. Shin, H. Ko, I.-K. Han, B.-K. Ju, S.-H. Kwon, D.-H. Ko, *Nano Lett.* **2015**, *15*, 2491.
- [189] J. B. Kerr, V. E. Fioletov, *Atmos. Ocean* **2008**, *46*, 159.
- [190] J.-S. Huang, M. D. Kelzenberg, P. Espinet-Gonzalez, C. Mann, D. Walker, A. Naqavi, N. Vaidya, E. Warmann, H. A. Atwater, in *2017 IEEE 44th Photovoltaic Specialist Conference (PVSC)*, IEEE, Piscataway, NJ **2017**, pp. 1248–1252.
- [191] I. Cardinaletti, T. Vangerven, S. Nagels, R. Cornelissen, D. Schreurs, J. Hruby, J. Vodnik, D. Devisscher, J. Kesters, J. D'Haen, A. Franquet, V. Spampinato, T. Conard, W. Maes, W. Deferme, J. V. Manca, *Sol. Energy Mater. Sol. Cells* **2018**, *182*, 121.
- [192] O. Malinkiewicz, M. Imaizumi, S. B. Sapkota, T. Ohshima, S. Öz, *Emergent Mater.* **2020**, *3*, 9.



Ram Datt is working as research staff in the SPECIFIC, Faculty of Science and Engineering, Swansea University, Swansea, United Kingdom. He completed his Ph.D. (2019) in Engineering Science from CSIR-National Physical Laboratory, New Delhi, India, in the field of organic solar cells. Currently, he is working on organic and perovskite solar cells for indoor and space applications and downconversion materials for photovoltaic application.



Swati Bishnoi is working as a postdoctoral fellow in Indian Institute of Technology (IIT) Delhi, India. She completed a Ph.D. in engineering science from CSIR-NPL, New Delhi, in 2018. She is working in the area of luminescent nanomaterials, downconversion, upconversion phosphors, and quantum dots for achieving the spectral conversion for photovoltaic application.



Sandeep Arya is a senior assistant professor in the Department of Physics, University of Jammu, India. He has more than ten years of research and teaching experience. His research interests include the synthesis of nanomaterials for energy and sensing applications. He has more than 50 research papers published in various national and international journals of repute.



Vinay Gupta is working as an assistant professor in the Department of Physics at Khalifa University of Science and Technology (KUST). He has research interests in solid-state physics, organic and perovskite solar cells, supercapacitors, lithium-ion batteries, and water filtration. He is a recipient of several international and national awards, including the prestigious Shanti Swarup Bhatnagar (SSB) award (2017) and Thomson Reuters India citation award (2015).



Wing Chung Tsoi is an associate professor at the Faculty of Science and Engineering, Swansea University, Swansea, United Kingdom. He obtained his Ph.D. from the University of Hull. His research interests include organic and perovskite photovoltaic cells for indoor and aerospace applications, organic semitransparent solar cells, their stability, and advanced characterization techniques to study optoelectronic devices. He has published 74 papers, given 33 invited talks, and was awarded the 2021 Royal Microscopy Society Medal for Innovation in Applied Microscopy for Engineering and Physical Sciences.